SENSITIVITY OF THE SHiP EXPERIMENT TO HIDDEN PARTICLES AT THE CERN SPS

A THESIS SUBMITTED TO
THE GRADUATE SCHOOL OF NATURAL AND APPLIED SCIENCES
OF
MIDDLE EAST TECHNICAL UNIVERSITY

BY

ATAKAN TUĞBERK AKMETE

IN PARTIAL FULFILLMENT OF THE REQUIREMENTS
FOR
THE DEGREE OF MASTER OF SCIENCE
IN
PHYSICS

NOVEMBER 2020

Approval of the thesis:

SENSITIVITY OF THE SHiP EXPERIMENT TO HIDDEN PARTICLES AT THE CERN SPS

submitted by **ATAKAN TUĞBERK AKMETE** in partial fulfillment of the requirements for the degree of **Master of Science in Physics Department, Middle East Technical University** by,

Prof. Dr. Halil Kalıpçılar
Dean, Graduate School of **Natural and Applied Sciences** _____

Prof. Dr. Altuğ Özpineci
Head of Department, **Physics** _____

Prof. Dr. Ali Murat Güler
Supervisor, **Physics, METU** _____

Examining Committee Members:

Prof. Dr. Orhan Çakır
Physics, Ankara University _____

Prof. Dr. Ali Murat Güler
Physics, METU _____

Prof. Dr. Altuğ Özpineci
Physics, METU _____

Prof. Dr. İsmail Turan
Physics, METU _____

Assoc. Prof. Dr. Deniz Yılmaz
Physics Engineering, Ankara University _____

Date:

I hereby declare that all information in this document has been obtained and presented in accordance with academic rules and ethical conduct. I also declare that, as required by these rules and conduct, I have fully cited and referenced all material and results that are not original to this work.

Name, Surname: Atakan Tuğberk Akmete

Signature :

ABSTRACT

SENSITIVITY OF THE SHiP EXPERIMENT TO HIDDEN PARTICLES AT THE CERN SPS

Akmete, Atakan Tuğberk
M.S., Department of Physics
Supervisor: Prof. Dr. Ali Murat Güler

November 2020, 80 pages

New Physics (NP) can be explored by connecting the Hidden Sector to the Standard Model (SM) through new (hidden) particles, which are very feebly interacting and have masses below the Fermi scale. The SHiP (Searching for Hidden Particles) experiment aims to search for hidden particles produced by transferring SPS proton beams into the Beam Dump Facility (BDF)'s fixed-target. In this thesis, the SHiP's sensitivity to two hidden particles, Dark Photon (DP) and Axion-Like-Particle (ALP), is studied. In order to achieve this goal, a chain of *physics implementation-MC grid production-sensitivity analysis* is composed, which is used to exclude a phase-space contour with a 90% confidence level. The results show that SHiP promises unique sensitivity regions which have not been investigated or considered previously.

Keywords: CERN, SPS, BDF, SHiP, Dark Photon, Axion-like Particle, Monte Carlo Simulation

ÖZ

CERN SPS'TE SHiP DENEYİNİN SAKLI PARÇACIKLARA HASSASİYETİ

Akmete, Atakan Tuğberk
Yüksek Lisans, Fizik Bölümü
Tez Yöneticisi: Prof. Dr. Ali Murat Güler

Kasım 2020 , 80 sayfa

Yeni Fizik (NP), çok zayıf bir şekilde etkileşime giren ve Fermi ölçeğinin altında kütlelere sahip olan yeni (saklı) parçacıklar aracılığıyla Saklı Bölümü Standart Modele (SM) bağlayarak keşfedilebilir. SHiP (Saklı Parçacıkların Aranması) deneyi, SPS proton ışınlarının Demet-Yığını-Tesisleri (BDF)'nin sabit hedefine aktarılmasıyla üretilen saklı parçacıkları aramayı amaçlamaktadır. Bu tezde SHiP'in iki saklı parçacığa, Karanlık Foton (DP) ve Aksialiyon-benzeri-Parçacığa (ALP) duyarlılığı incelenmiştir. Bu amaca ulaşmak için, bir faz-uzay sınırını dışlamak için kullanılan bir *fizik uygulaması - MC örgü üretimi - hassasiyet analizi* zinciri oluşturulur %90 güven düzeyiyle. Sonuçlar SHiP'in daha önce araştırılmamış veya dikkate alınmamış benzersiz hassasiyet bölgeleri vaat ettiğini göstermektedir.

Anahtar Kelimeler: CERN, SPS, Demet Yığını Tesisi, SHiP, Karanlık Foton, Aksion benzeri Parçacık, Monte Carlo Simulasyonu

I dedicate this thesis to my parents, my wife,
and everyone who will benefit from this work.

ACKNOWLEDGMENTS

During this thesis, among the numerous experiences, I got the first impressions of doing research, and I learned the importance of collaborations and communication. I had the chance to investigate unexplored regions in the particle physics.

First of all, I want to express my gratitude to my principal investigator, Prof. Dr. Ali Murat Güler. He opened his lab to me in my last year BSc education. He gave me his full support to express myself and follow my enthusiasm. He provided me with the chance to work on this project at SHiP, CERN. Furthermore, he listened to me and advised me in every step of the studies, about life and career. He taught me everything I know about computational physics, statistics, and experimental particle physics. More than these, I learned to present my studies and to be a researcher. He encouraged me to pursue my path and how to work in collaborations. He always respected my opinions; he listened to them carefully, and he contributed the best feedback. I was so lucky to have him as an advisor. It is thanks to him that I will continue on this journey.

I want to thank my valuable jury members for their feedback during my defense procedure. I cannot express how much I am grateful to have them on my thesis committee.

I want to thank Prof. Dr. İsmail Turan, whom I met during his BSc elementary particle physics course. He corrected me about the theoretical sections and asked me questions, which helped me better understand the theoretical part of my work. I thank Prof. Dr. Altuğ Özpineci for his valuable criticism of fundamental physics during the defense. I also thank Assoc. Prof. Deniz Yılmaz for his support in my stressful times during the defense and his advice about my next steps in my future career. I would like to thank the jury president, Prof. Dr. Orhan Çakır, for making me think about the technical details of the MC generators in the thesis.

I also want to give my most profound appreciation to the SHiP collaboration in my first research experience. The collaboration provided the best sources, experts, and facilities of CERN.

DP team leader and my mentor on my first project, Anne Marie Magnan, guided me through the DP sensitivity search publication. She taught me a great deal about physics simulations and sensitivity analysis. She showed me how to express my results adequately and how to make publications. Her professionalism was an example to me. Even when I got stuck, she explained to me every detail patiently. I will always remember and be thankful for all the inspiring conversations we had. I would like to thank our software manager, Thomas Ruf, who is the main contributor to Fairship. He gave his technical support in FairShip; he provided me the best tools in DP analysis and cascade studies, helped me understand the physical meaning of the codes, assisted me in the implementation of ALPACA, and checked and questioned me on every step from production to analysis. I also want to thank our technical coordinator, Richard Jacobsson, for giving me the chance to present my updates during the JPD meeting sessions, providing his valuable feedback, conducting me with other experts, and explaining my study's phenomenological details whenever I needed it. The SHiP Country Representative Board chair, Eric Van Herwijnen, gave me full responsibility for the muon-flux test-beam measurement during my shifts. Moreover, he helped me during my Ph.D. application and provided me the options that I should consider. I give my sincerest appreciation and gratitude to him. I would like to thank our conferences and publication board chair, Walter Bonivento, for his help and guidance during the publication procedure of DP sensitivity analysis. He advised, asked, and forced me to ask myself what I want to do through the career of high energy physics. I also thank the SHiP Physics Planning group chair, Nicola Serra, who gave me this chance without doubt and the utmost credit in every possible situation. I also want to thank the internal referees of DP publication, Antonia Di Crescenzo and Oleg Ruchayskiy, for their vital inputs. I want to also thank Oliver Lantwin for helping me with the essential techniques and methods on the computational side and assisting me during the ALPACA implementation. I will always be grateful to have such a friend and colleague.

Middle East Technical University has given me the opportunity to be part of a successful laboratory, Prof. Dr. Guler's High-Energy-Physics laboratory. I cannot tell how much I am lucky to have this working group.
My dearest friend since the first year of BSc, Onur Durhan, always helped me whenever I need it without hesitation. We spent countless hours at CERN and METU libraries. Even in the defense process, he was always there to support me. I cannot express how much I am grateful to him. I thank my other team member, Enes Tepe, for introducing me to the group and encouraging me to join the group. I also thank my other lab members, Muhteşem Akif Korkmaz, Emircan Elikkaya, and Nilay Bozdağ.

I also want to mention my family, who always wants me to dedicate myself to what I enjoy and what makes me happy. They gave their best efforts for me to have the best education.

My wife, Sara Mingu-Akmete, was always there and helped me to improve myself. She saw the best in me, and encouraged me to believe in myself, listened to me many times. Her wisdom on life and work ethics impressed me and was an example. She proofread my presentations and reports, and she taught me how to improve them. We spent so many days and nights on our projects, shoulder to shoulder. I hope we will do much better together in the future.

I gratefully acknowledge TAEK for supporting our project "Testing Beyond the Standart Model Theories at CERN and Development of Emulsion Based Detectors" (project no: 2018TAEK(CERN)-A5.H6.F2-17).

TABLE OF CONTENTS

LIST OF TABLES

TABLES

LIST OF FIGURES

FIGURES

LIST OF ABBREVIATIONS

SHiP	Searching for Hidden Particles
SM	Standard Model
BSM	Beyond the Standard Model
HS	Hidden Sector
DP	Dark Photon
ALP	Axion-like Particle
QCD	Quantum Chromodynamics
QFT	Quantum Field Theory
QED	Quantum Electro Dynamics
MC	Monte Carlo
FT	Fixed Target
BDF	Beam Dump Facility
NP	New Physics
BR	Branching Ratio
FT	Fixed-Target
LHC	Large Hadron Collider
SPS	Super Proton Synchrotron
BDF	Beam Dump Facility
HNL	Heavy Neutral Lepton
SND	Scattering and Neutrino Detector
CERN	The European Organization for Nuclear Research
2D	Two Dimension
vtx	Vertex
P8	Pythia8

G4	Geant4
reco	Reconstruction
pbrem	Proton Bremstrahhlung

CHAPTER 1

INTRODUCTION

At the beginning of the 1930s, the picture of *elementary particles* still resembled a stable atomistic model, and it did not involve fields and charges. Until the 1970s, this picture evolved into its current form due to the development of the Standard Model (SM) and the Quantum Field Theory (QFT) through many experiments and theorems. QFT interpretation of SM suggests describing the elementary particles and their interactions by symmetry groups [2–5]. Later, unique dedicated experiments tested the predictions of SM. This effective formulation was confirmed by discoveries such as W and Z bosons in 1983 and the famous Higgs boson in 2012 at CERN [6–11]. Finally, SM was completed, which explains the fundamental physics, except gravitational forces, with a high level of precision [12–15].

Although SM is a well-established theory, its limits are still under investigation. Moreover, SM fails to answer particular issues such as the existence of Dark Matter and Energy, baryon asymmetry of the universe, and neutrino mass and oscillations. New Physics (NP) solutions to these enigmas are referred to as physics "Beyond the Standard Model" (BSM). BSM solutions may be provided by extending the SM with the least amount of new particles and interactions [16–19]. A straightforward BSM strategy would be to investigate new particles by increasing the energy limits of accelerators [16–18]. Many collider experiments are already designed as *high energy frontiers*, and they look for new heavier particles. Similarly, *cosmic-frontier* experiments could also examine the new heavier particles if they interact relatively feebly. The new heavier particles may require extra dimensions and corrections in the SM [20, 21]. However, new particles can have masses up to the Fermi scale,

with very small couplings [17]. In that case, the experiments of energy-frontiers and cosmic-frontiers have the lack of a clean environment to detect the new particles [18, 19]. Another possible BSM strategy is a (hidden) sector with new fields with renormalized interactions, which stays hidden (uncharged) to the SM at very low energies. Nonetheless, the *hidden sector* (HS) can have feeble interaction (charge) with the *SM Sector* below the Fermi scale; this interaction would be mediated by the notion of *portals*. In that instance, the mixing of HS with SM can be possible through lighter portal particles (messengers), and this phenomenon might indicate NP with a new energy scale [20]. BSM searches from the portal particles again would require a reduced background [21, 22]. Such experiments, which aim to obtain more interaction with less background instead of reaching higher energies, are referred to as *intensity-frontier* experiments. The comparison between intensity and energy frontier experiments in the BSM problems is illustrated in Figure 1.1. The full investigation of BSM requires the combinations of the three frontiers; in particular, the intensity-frontier experiments which use intense beams on high-density fixed-targets promise more answers (see Figure 1.2).

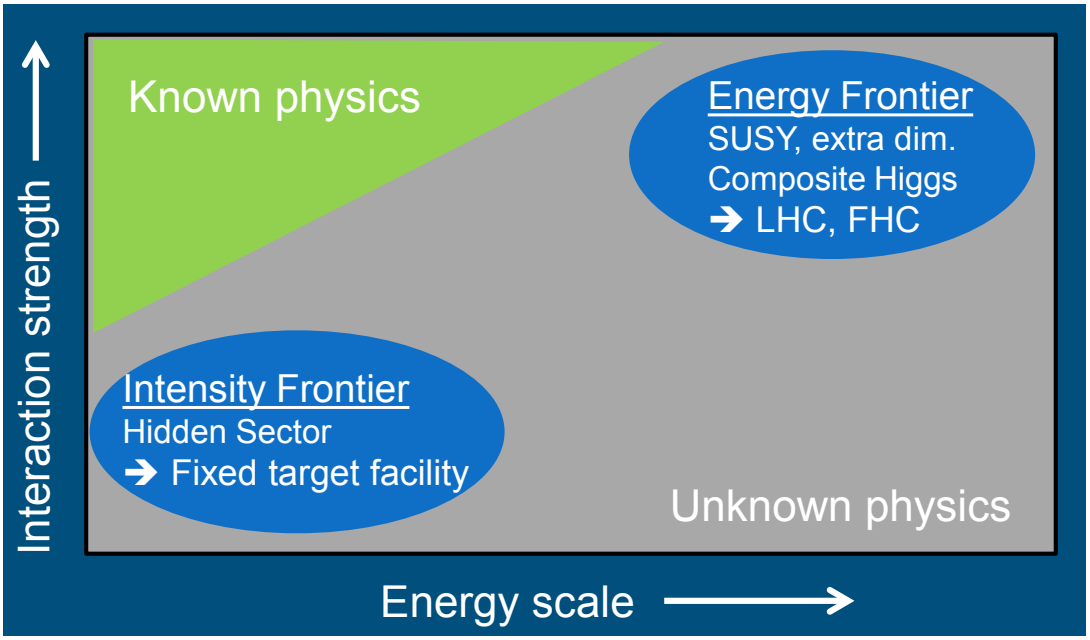

Figure 1.1: BSM searches are described as a function of intensity strength and energy scale.

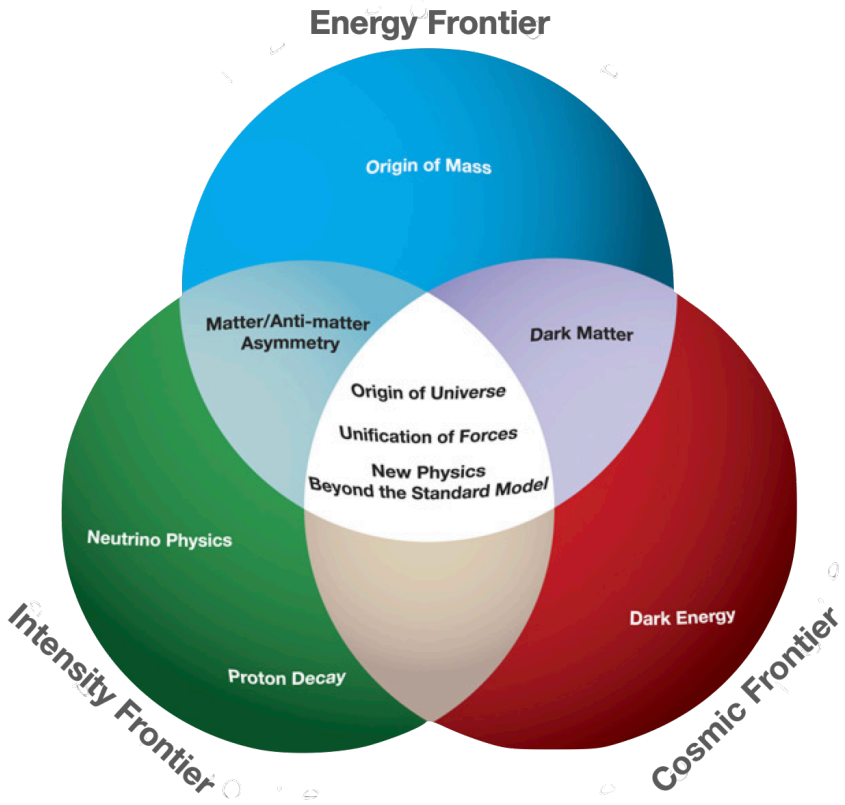

Figure 1.2: Possible research topics at the three frontiers.

The SHiP (Searching for Hidden Particles) experiment at CERN-SPS is proposed [23] to search for the light hidden particles with zero background. In five years of data taking, CERN-SPS will provide 2×10^{20} protons on target through Beam Dump Facility(BDF) [24]. SHiP can search for any new feebly interacting particle with mass below $\mathcal{O}(10$ GeV). Since SHiP has a dedicated neutrino detector, a reach neutrino physics program can be performed in addition to hidden particle searches. SHiP will employ a 120-meter long setup, whose most crucial parts are a 35-meter active shielding and a 50-meter long decay vessel. BDF is a new proposed facility at CERN SPS, with the aim of hosting fixed-target experiments such as SHiP, which will be the first experiment to take place at BDF. For the moment, BDF and SHiP are in the R&D phase as a part of the Physics Beyond Collider (PBC) forum [19]. The SHiP Comprehensive Design Study (CDS) Report [25] and BDF Comprehensive Overview [26] have been submitted to EPPS (European Particle Physics Strategy); their outcomes have been summarized in the SHiP Progress Report [18] and sent to

the SPS-committee. In light of this, this thesis presents the SHiP detector sensitivity to the dark photon model of the vector portal. The results have been used in the SHiP proposals and finalized in a publication [27]. Additionally, the MC-level sensitivity of SHiP to the axion-like-particle model of the higher dimensional portal is included in the thesis.

The structure of the thesis is as follows:

- **Chapter 2** gives a concise explanation of the SM and beyond. It then introduces NP direct search by linking the HS to SM through portals in intensity-frontiers.
- **Chapter 3** provides an overview of the SHiP experiment's motivation, setup and software framework.
- **Chapter 4** summarizes the theory of dark photon, with its production and decay mechanisms. Moreover, this chapter gives the MC production and analysis to evaluate the SHiP sensitivity to the dark photon.
- **Chapter 5** presents a description of the diphotonic coupled axion-like-particle. It provides the MC simulation and analysis, which are then used for obtaining the SHiP sensitivity to the axion-like-particle.
- **Chapter 6** provides the SHiP exclusion contours to the two hidden particles and concludes possible outcomes.

CHAPTER 2

EXPLORING HIDDEN PARTICLES

2.1 The Standard Model and Beyond

The gauge structure of SM as a quantum field theory provides a precise explanation of the fundamental interactions of EM, Weak and Strong forces, together with the elementary particles. The elementary particles in SM are separated into two groups according to their spin: spin-1/2 fermions, which form matter, and spin-integer bosons, which are force mediators. Fermions are classified into two groups, namely leptons and quarks, each of which is further divided into three generations. Each lepton generation consists of one electrically (-1) charged lepton and one electrically neutral lepton: the electron e^- with the electron neutrino ν_e, the muon μ^- with the muon neutrino ν_μ, and the tau τ^- with the tau neutrino ν_τ. Similarly, each generation of quarks consists of one electrically (+2/3) charged up-type quark and one electrically (-1/3) charged down-type quark: namely, up (u) and down (d), the charm (c) and strange (s), the top (t) and bottom (b) quarks. There is also an associated antiparticle with the same mass but opposite charge for each of these fermions. Quarks can not be isolated (free); they form bound states, which are called hadrons. They are classified into two groups:

- Baryons, consisting of three quarks,
- Mesons, consisting of one quark and one antiquark

Baryons are composed of three different colored quarks; their net color charge is neutral. Likewise, antibaryons are composed of three different anticolored antiquarks;

their net color charge is also neutral. In mesons, quarks and antiquarks have the same color and anticolor, and hence they are colorless. Thus, all free particles have neutral color charges.

A conserved quantum number, called the baryon number (B), can be defined for hadrons. B is +1 for baryons, and -1 for the antibaryons, +1/3 for quark, -1/3 for antiquarks, and 0 for the mesons. Another conserved quantum number is the lepton number (L). For electrically (-1) charged leptons and their left-handed neutrinos, L is +, while for electrically (+1) charged antileptons and their right-handed antineutrinos, L is -1. The pairs of particle-antiparticle annihilate to bosons, e.g., electron-positron pairs annihilate to photons.

In physics, symmetric means being invariant, or remaining unchanged, under some transformation that yields a conservation law. In particular, charges are conserved quantities under internal (or local) symmetries. Internal symmetries are transformations that act on local fields, and they have nothing to do with space-time translation. They make the interactions invariant under the gauge transformations* that make charges conserved, e.g., invariance of EM under gauge transformations leads to a conversation of Q charges. Hence, internal symmetries can correlate the same type of particles, e.g., isospin for protons and neutrons, to form a doublet that will be a single particle, the nucleon. These types of internal symmetries are known as flavor symmetries. For quarks, flavor symmetries will be easier to work with; u and d quarks also form a SU(2) doublet. As in the case of nucleons, these two quarks have similar masses as well. They also give rise to SU(3) triplet with the s having different mass.

Another important transformation is the parity inversion, which transforms a phenomenon into its mirror image. The fundamental interactions, except for the weak interaction, are symmetric under parity. For massless particles, chirality and helicity are the same: negative helicity particles are left handed, positive helicity particles are right handed. Both of these quantities are conserved for a free particle and they are frame independent. For massless particles, helicity is still conserved for free parti-

* gauge refers to any mathematical formalisms to regulate redundant degrees of freedom in the Lagrangian, and the transformations between gauges, gauge transformations, form a symmetry group, which can explain elementary particles and their interactions

cles, but since the particle moves at speeds slower than the speed of light, it is not frame independent. Chirality on the other hand is not conserved for a massive free particle, but it is frame independent. Only left-handed fermions and right-handed antifermions participate in the charged weak interaction. The neutral weak interaction of the left-handed fermions is dominant over right-handed fermions; this issue violates the parity transformation. Left-handed fermions have isospin, T = 1/2, and they make doublets with $T_3 = \pm$ 1/2, which act the same in weak interaction. The sign of T_3 of electrically charged fermions is the same as their electric charge. Thus, T_3 = +1/2 for the $(\mathrm{u}, \mathrm{c}, \mathrm{t})$ quarks transformed into $(\mathrm{d}, \mathrm{s}, \mathrm{b})$ quarks with T_3 = -1/2, and vice versa. Furthermore, a quark does not transform weakly into the same T_3 quark. For the leptons; e^-, μ^- and τ^- have T_3 = -1/2, while ν_e, ν_μ and ν_τ are with T_3 = +1/2. Likewise, the antifermions have reversed sign in T_3 and right-handed chirality. $T = T_3 = 0$ for the right-handed fermions and left-handed antifermions, and they form SU(2) singlets. The remaining is the weak hypercharge, Y_W:

$$Q = T_3 + \frac{1}{2} Y_{\mathrm{W}}$$

In short, B, L, Q, T_3 and Y_W are conserved internal charges of the three fundamental interactions that are invariant under the gauge transformations of the $SU(3)_C \times SU(2)_L \times U(1)_Y$:

- **Electromagnetism** is invariant under the unitary $U(1)_{EM}$ symmetry. The massless vector boson of the $U(1)_{EM}$, photon (γ), is described by the $U(1)_Y$ and one of the doublet $SU(2)_L$. EM interaction ranges to infinity, i.e., galactic magnetic fields $\geq 10^{17}$ km. Photons can produce electron-positron by interacting with the nuclei's electric field. Inversely, the annihilation of electron-positron to two photons is called annihilation of matter.

- **Weak interactions**: Massive gauge bosons of the weak interaction are $W^{\pm}$ and Z. They become massive by Higgs during symmetry breaking. Furthermore, $W^{\pm}$ are the only electrically charged bosons.

- **Strong interactions**: The combinations of a color and an anticolor in the symmetry group SU(3) would give eight (3^2 - 1 = 8) massless vector (spin-1) bosons, gluons (g), as mediators to the strong interaction. They give asymptotic

freedom to quarks; together, they bound the hadrons. Moreover, some neutral mesons, such as neutral pions and neutral kaons, can be the strong interaction mediator bosons between hadrons, i.e., the bound of protons and neutrons in the nuclei. For this reason, the strong force refers to a nuclear force, and it acts over shorter distances. The leptons are not confined, and they do only electroweak interactions.

The scalar boson, Higgs, H, gives mass to the particles (except for the neutrinos), leading to a spontaneous symmetry-breaking. Notably, two of the fundamental interactions, EM and Weak, are unified in the broken hypercharge gauge symmetry (see Figure 2.1). In the spontaneous symmetry breaking, the equations of motion are invariant, but not the system itself. The background of the system (vacuum) is not invariant since the vacuum is a collection of all ground states.

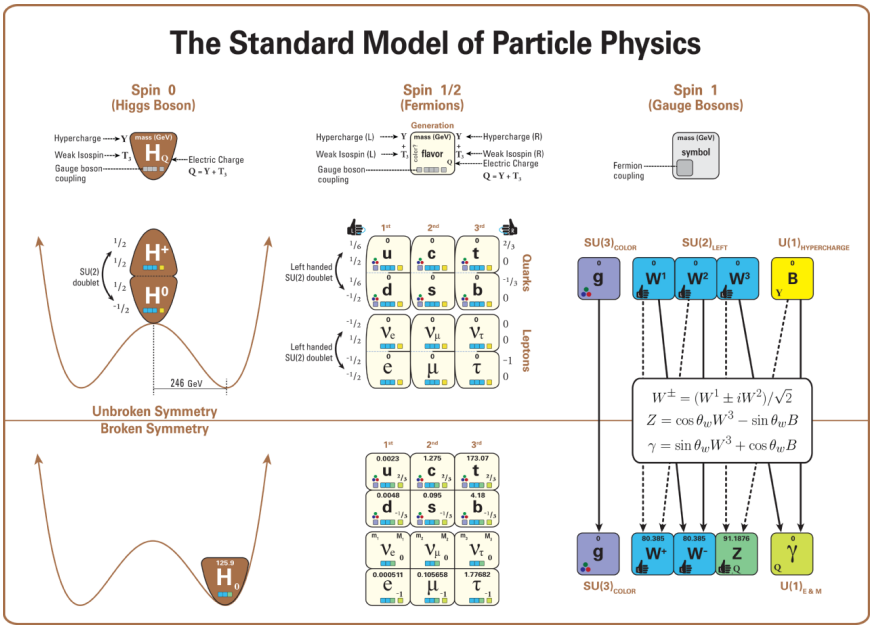

Figure 2.1: (Un)broken symmetries of the Standard Model

To conclude, SM is a consistent gauge theory. It means that SM remains unchanged under the specific symmetry transformations that lead to introduce other groups. Nevertheless, SM has some problems which may not be solvable with its framework, which would require approaches beyond this model. These problems are described

below:

- Baryon asymmetry of the universe (BAU): there is an asymmetry between matter and antimatter. If the initial baryon number of the universe is assumed to be zero at the time of the Big Bang, then it should have remained zero. However, antimatter annihilated with the matter, and the matter somehow became dominant by nucleons.

- Existence of neutrino masses and oscillations that are neglected in the SM; neutrinos oscillate by mixing between the flavor and mass eigenstates. The three neutrino states that interact in weak force with the charged leptons are different superpositions of the three propagating neutrino states of definite mass. Even though neutrinos are emitted and absorbed in weak processes as flavor eigenstates, they travel as mass eigenstates.

- Evidence of DM and Dark Energy, which are abundant over known SM matters in the universe; first, DM was observed from the difference between the predicted and observed mass of the Coma cluster, indicating a missing mass that does not radiate through the SM charges. Then, the galaxies' measured rotation curves indicated that DM makes a spherical halo that covers the galactic nucleus. The first verification of Dark energy was obtained from supernova measurements, which showed that the universe expansion rate is accelerating. Without Dark energy, the expansion rate should decrease. Then, the cosmic microwave background (CMB) showed that the universe began in a hot Big Bang. These indicated the existence of new energy, Dark Energy.

2.2 Hidden Sector through Portals

Our knowledge about the universe's history has been developed recently by many observations and measurements. They lead us to assume that the universe has emerged after inflation and baryogenesis, but before Big Bang nucleosynthesis (BBN) and cosmic microwave background (CMB) radiation. Also, until now, the search for new particles at high-energies with larger couplings have not provided any positive results. In light of these, there might be a new neutral hidden sector(s) (HS) below the EW scale,

which can interact very weakly with the SM particles. They might have not been discovered yet due to their small couplings and energy scales [16–18, 18, 19, 26, 30, 31]. These new particles, hidden particels, with lighter masses below the EW scale can do their feeble couplings with the SM fields via renormalizable interactions with small dimensionless coupling operators. These operators are known as portals, and they can mediate dark (hidden) force between SM and HS while respecting the symmetries of SM. There are different types of portals coupling with the SM sector according to the spin of the mediator: scalar portal (spin-0), neutrino portal (spin-1/2), vector portal (spin-1), and a particular case of a non-renormalizable model with small coupling (has a unit of GeV^{-1}) predicting spin-0 axion-like particles (ALP) that decay into fermions and gluons [1, 32–36]. They are tabulated in Table 2.1) along with their interaction types.

Table 2.1: Portals with their interactions

Portal	Interaction
Scalar (Dark Higgs)	$\left(H^\dagger H\right)\phi$
Vector (DP)	$\epsilon F_{\mu\nu}F'_{\mu\nu}$
Fermion (Heavy Neutral Lepton (HNL))	$H^\dagger \bar{N} L$
Higher-dimensions (ALP)	$aF^{\mu\nu}\tilde{F}^{\mu\nu}$

Since we are free to add new groups to SM, we can use this freedom for the connection between HS ($\mathcal{L}_{\mathrm{HS}}$) and SM ($\mathcal{L}_{\mathrm{SM}}$) through *portal* ($\mathcal{L}_{\mathrm{portal}}$) with quantum numbers from two sectors:

$$\mathcal{L} = \mathcal{L}_{\mathrm{SM}} + \mathcal{L}_{\mathrm{portal}} + \mathcal{L}_{\mathrm{HS}}$$

The constraints on the direct coupling between known matter and dark matter are increasing, but descriptions of their dynamics are not valid. One possibility can be that DM interacts with SM via dark force [37–39]. The major hidden particle that we will be interested in is the Dark Photon (DP) of the vector portal, which is a dark force mediator between two sectors. Since all three forces of SM are mediated through

vector bosons, the vector portal should be the most highlighted. At the same time, we will investigate the ALP portal's potential, a higher dimensional portal with a pseudoscalar particle that mixes with the photon in the SHiP setup.

- **Vector Portal:** Supersymmetric models, superstring models, the grand unified theories, and the fifth force models predict an extra $U(1)'$ factor. Then, there can be an electrically neutral vector boson of the hidden abelian (commutative) symmetry group $U'(1)$. Furthermore, these vector particles are often grouped under the name of Dark Photon (γ^{D}). There are several DP models such as very light (*B* - *L*)[†] charged DP model [40] and Leptophilic gauge bosons which only couples with leptons. However, the DP model in which we are interested appears as relatively massive and, at the same time, as the lightest of the $U(1)'$. Hence it couples with SM through the kinetic mixing. This assumption can be used in superstring or supersymmetric models [41, 42]. The kinetic mixing model of DP is the most generic and minimalist one due to its ability to be explained by just two parameters. $\mathcal{L}_{\mathrm{mix}}$ is given by

$$\sim \varepsilon F'_{\mu\nu} F_Y^{\mu\nu} \tag{2.1}$$

  where ϵ is the kinetic mixing term, $F'_{\mu\nu}$ is the field of the $U(1)'$ and $F_{\mu\nu}$ is the field of the $U(1)_Y$

- **Higher-dimensional Portal:** Axions are introduced in a new Peccei-Quinn global broken $U(1)$ symmetry, $\tilde{U}(1)$ or $U(1)_{PQ}$, as a solution to the CP problem. Axions are well motivated DM candidates that can solve the CP problems of QCD. Massive axions can be produced in the early universe, and they can be generalized under the String theory. They have higher dimensional and non-renormalizable coupling to the SM. The minimalist higher-dimensional model with mass and coupling term with GeV^{-1} is massive ALP. They are Pseudo Nambu-Goldstone Boson (PNGB) of a new (not exact) spontaneous symmetry breaking. The pseudoscalar field, a, can be used to write its mixing with quarks, leptons, photons, and other SM fields. Between those coupling types, we only

[†] In the grand unified theory (GUT), baryon and lepton number conservation can be violated if the difference between them (B - L) is conserved.

consider the photon dominance mode; the whole model, its production and decay, would be explained by two free parameters, m_a and $g_{a\gamma}$. Those ALPs, pseudoscalar axion-like particles, couple to four-dimensional two-photon operators [1, 29, 32, 35, 36, 43]. $\mathcal{L}_{\rm mix}$ is given as:

$$g_{a\gamma} a F^{\mu\nu} \tilde{F}_{\mu\nu} \tag{2.2}$$

where $\tilde{F}_{\mu\nu}$ is the field of the $\tilde{U}(1)$ and $F_{\mu\nu}$ is the field of the $U(1)$. The effective coupling to two photons is $g_{a\gamma} \sim \frac{\alpha}{2\pi F}$. Then, the coupling and the mass are determined by F. It ranges between 10^9 and 10^{17} GeV in the case of the string theory, supernova SN1987A excludes F smaller than 10^9 GeV. Meanwhile, future experiments promise F equal to or smaller than 10^9 GeV, or F equal to or bigger than 10^{12} GeV [28]. Hadron coupled PNGBs were studied in proton and electron beam dumps in the 80s; CHARM at CERN, SLAC experiments of E137 and E141, and E774 at Fermilab are the remarkable ones. Such limits are also calculated in the kinetic mixing bosons, i.e., DP [44].

2.3 Investigation of NP at Intensity-Frontier Experiments

Even though LHC still has a good deal of discovery potential, particle physics must examine all possible domains cautiously. Furthermore, since the discovery of the Higgs boson, no new particle has been detected. Besides the failures on direct NP searches, several precision measurements have been made to search limits of SM, such as LHCb and Belle, and they have reported the violation of the lepton flavor universality in semi-leptonic B decays. However, still, there is no direct observation of NP. This lack of direct evidence can be explained by the assumption of too feeble new particles. Searching for feeble interacting particles in the MeV-GeV range is challenging; however, it promises a novel exploration to the HS [35]. The current and future proton beam-dump facilities with a high-beam intensity and energy will be suitable to search for very feebly interacting particles in the mass range between MeV and GeV [1]. The hidden particles may decay into SM particles very feebly in a lifetime of $\mathcal{O}(10)$ meters [44]. Intense proton-beams are available, and together with sensitive detectors, they will allow for more robust and sensible investigations [18, 19, 25, 32]. Fixed-dense-proton-target experiments with a long decay vacuum are the perfect op-

tion to explore those weakly coupled sectors; however, there are not many beams nor detectors for this kind of research [1, 17, 18, 25, 35, 44]. The bosons (spin-0 and spin-1) can radiate in the intense-particle interactions among matter proportionally to the square of their weak coupling with a nominal rate [16–19, 44]. As a result, this will be a good opportunity for the fixed-target experiments to discover NP, or, at least, to complement collider experiments. Moreover, they can expand their sensitivitive regions as the power of beams goes to the megawatts [32]. Meanwhile, the low-energy experiments, e.g., Belle-II, and collider experiments, e.g., FASER [33] at LHC, should be run in parallel [35].

CHAPTER 3

THE SHIP EXPERIMENT

3.1 Motivation

The detection of the Higgs boson marked the completion of the guaranteed discoveries of particle physics. SM was thus verified as a self-consistent and an effective field theory, up to the scale of quantum gravity, the Planck scale [17, 18, 45–50]. Interestingly, mass values of top-quark and Higgs boson are close to the EW symmetry breaking. Moreover, due to the observed phenomenons of BSM, SM does not represent the complete picture. These point to the existence of new physics (NP). Nevertheless, there is no certain clue about where to find NP, nor any information about the masses, coupling terms, and spins of the NP particles. Even though pp collisions at a center-of-mass energy of 13 TeV have been reached, there has been no significant deviation from SM. Although NP searches have not provided any positive results, searches are going on at the energy frontier with innovative detection strategies. On the other hand, the lack of neutrino masses and oscillations. The lack of observations in direct and indirect search experiments of weakly interacting massive particles (WIMPs) in the GeV-TeV mass range directed our attention to the lower-energy experiments. In summary, this current picture of particle physics suggests: NP could be either heavier beyond today's accelerators or interact very feebly. Therefore, there is a need for complementary searches like [18]

- **The direct searches in energy-frontier** at untested high-energies at laboratories.
- **The indirect searches on precision-frontier** to find failures of SM with high-precision experiments regardless of the energy scales.
- **The direct searches on intensity-fronties** to extremely feebly interacting relatively new light particles.

There are a lot of searches at the energy frontier such as LHC experiments and at the precision frontier such as LHCb experiment; however, the intensity-frontier remains under-explored. The motivation of the SHiP experiment is to make a break-through discovery at the intensity-frontier. Therefore, SHiP aims to explore the domain of particle masses and couplings, which are not accessible to the energy and precision frontier experiments. Furthermore, it has a possibility to look for light HS in GeV-scale with luminosities several orders of magnitude larger than energy-frontiers. Since the large forward boost gives good acceptance despite the smaller angular coverage, SHiP is sensitive to all these portals in Table 2.1. SHiP can also probe the existence of LDM through the observation of its scattering off electrons and nuclei in the detector material. Besides that, SHiP provides an indirect search to HS as a precision experiment by tau neutrino physics and neutrino-induced charm production. In the wake of the SHiP experiment, other dedicated intensity-frontier experiments have been proposed in recent years. This led to the creation of a dedicated study group of PBC [19] by the CERN management in 2016. Thus, in 2016, the CERN Management created a dedicated study group PBC [19]. However, among many proposed experiments interested in direct searches of HS, SHiP remains a unique dedicated experiment capable of reconstructing the decay vertex of an HS particle, measuring its invariant mass, and providing particle identification of the decay products in an environment of extremely low background.

3.2 Setup

The SHiP experiment aims at reducing the beam-induced background to 0.1 events in the 2×10^{20} protons on target. The SHiP will collect an annual yield of 4×10^{19} protons on target with a beam momentum of 400 GeV while respecting the HL-LHC beam requirements. Currently, CERN has no experimental facility compatible with this beam power. To meet SHiP's objective, the experimental set-up (see Figure 3.3) includes a set of magnets to deflect muons emerging from the target and a vacuum vessel to reduce the number of neutrino interactions in the decay volume. The target and the first part of the muon shielding will be handled by Beam Dump Facility [26]. SHiP/BDF is planned to be installed in the TT20 transfer line at the North Area, SPS, CERN (see Figures 3.1 and 3.2).

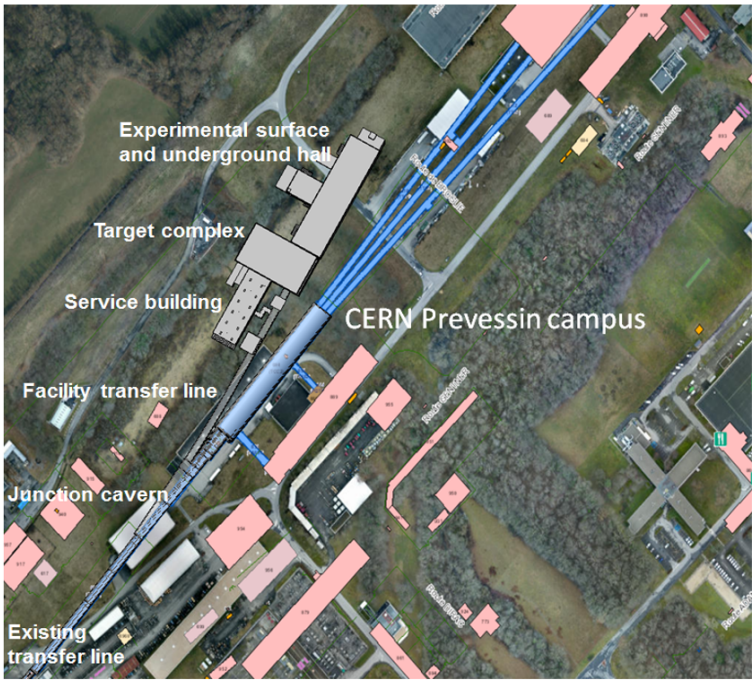

Figure 3.1: Location of the facility

The set-up consists of the proton target located before a hadron absorber, which is then followed by a unique muon shield [51, 52] to sweep the muons produced in the beam.

The target has to safely absorb the full 400 GeV/c SPS primary beam every 7.2 sec-

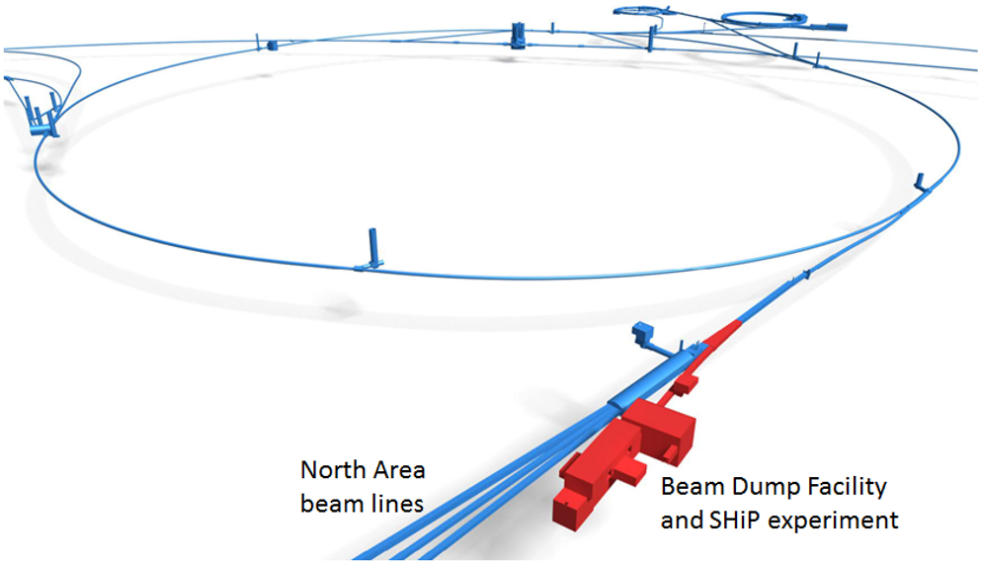

Figure 3.2: Layout of the SPS beam extraction to SHiP/BDF

onds. It is required that the target maximizes the production of charm and beauty hadrons and the re-absorption of pions and kaons. This implies a high-Z material with a short nuclear interaction length. The target is made of blocks of a titanium-zirconium doped molybdenum alloy (TZM) in the core of the proton shower, followed by blocks of pure tungsten with a tantalum cladding. The total target thickness is twelve interaction lengths. The production cross-sections of the GeV-scale hidden particles with small couplings are achieved by a factor of Z^2 in a heavy nucleus

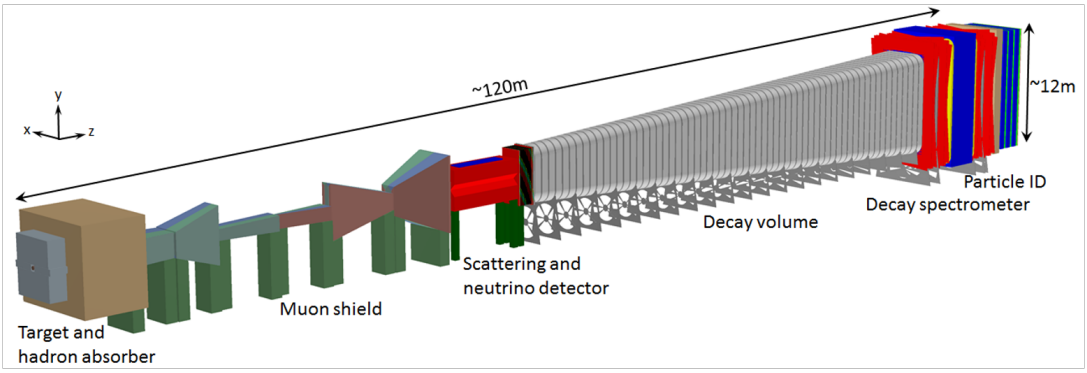

Figure 3.3: Overview of the SHiP experimental facility.

fixed-targets such as Molybdenum [53] (see Table 3.1). The high-density targets with intense proton beams would give energetic mesons and strong interactions.

Table 3.1: Molybdenum's atomic mass and the interaction length

Atomic mass	95.95 gmole^{-1}
Nuclear interaction length	155.8 gcm^{-2}

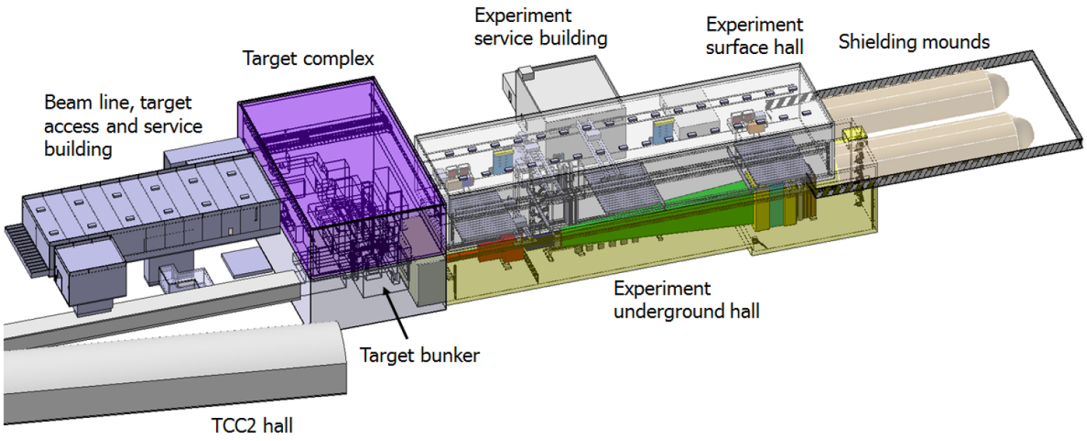

Figure 3.4: Planned facility layout

Two complementary detectors are incorporated into the SHiP detector; the Scattering and Neutrino Detector (SND), and the Hidden Sector (HS) spectrometer.
The SND will search for LDM scattering and perform neutrino physics searches. The SND magnetic spectrometer will allow for the first time to distinguish between ν_τ and $\bar{\nu_\tau}$ interactions by measuring the charge of τ decay products.

The HS decay volume (shown in Figure 3.5) is surrounded by a background tagger (SBT), and it is followed by the HS spectrometer. The decay volume should be located in close proximity to the target. Moreover, the target should have a short interaction length and be followed by the hadron absorber. The rationale behind these decisions is as follows:

- hidden particles that originate from charm and beauty are produced with a significant transverse momentum to the beam axis,

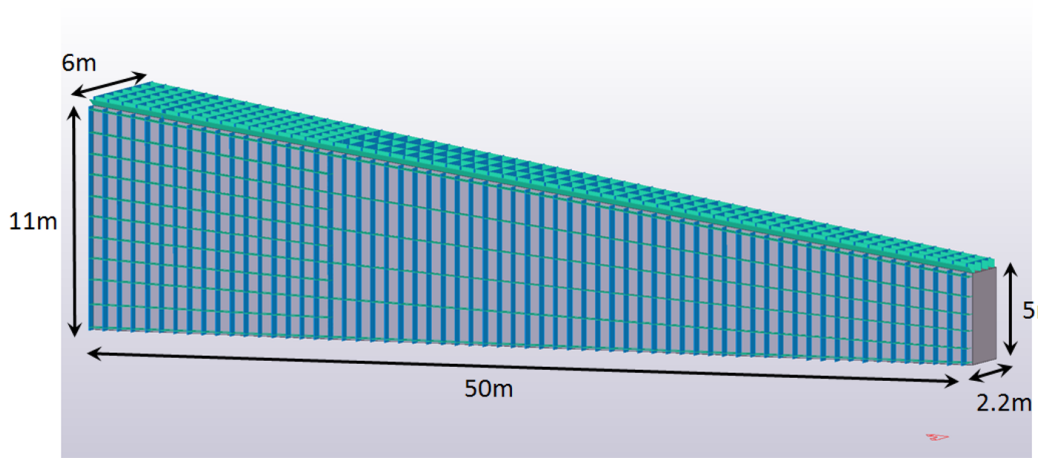

Figure 3.5: Schematic of decay vessel

- background is generated from the flux of produced muons and neutrinos,
- deep inelastic neutrino-nucleon scattering in the detector volume leads to background events through the production of V^0 particles whose decay mimic the topology of the hidden particle decays.

Due to the large production angle of hidden particles, the beam size is not important. However, several restrictions apply to the decay volume:

- The decay volume has a shape of the pyramidal frustum, and its length is ~ 50 m
- The structure is as light and as slim as possible in order to stay within the boundaries of the deflected muon flux while maintaining the required acceptance.
- In order to suppress neutrino-induced background events in the fiducial decay volume, the experiment vacuum vessel is kept at a pressure of 1 mbar.
- Its width is decided according to the shielding of the flux of muons. However, the high flux of muons produced by short-lived resonances and decaying hadrons such as pion and kaons would still give a severe background for the new physics searches.
- The SBT detects charged particles either entering the vacuum vessel from outside or produced in the inelastic interactions of muons and neutrinos in the

vacuum vessel walls.

The role of the muon shield (see Figure 3.6) is to deflect this flux away from the detector until the level of $\mathcal{O}(10^{-6})$. The muon shield and the SHiP detector will be placed in $\sim$ 120 m long underground experimental hall (see Figure 3.4) at a depth of $\sim$ 15 m. No infrastructures are placed to the detector to minimize the background induced by the flux of muons and the neutrinos interacting with the material. The muon shielding magnet is 35 m long and has 1300 T of magnets. The knowledge of the total charm production yield in 400 GeV proton interactions on the SHiP target is essential for the experiment, both in establishing the SHiP sensitivity to detect new particles and making a precise estimate of the tau neutrino flux produced in D_s decays. In order to validate the SHiP Monte Carlo simulation, the collaboration requested three weeks of beam time in 2018, the muon flux test beam (see Figure 3.7), intending to collect $\mathcal{O}(5\times10^{11})$ 400 GeV protons on target and accurately measure the muon flux emanating from the SHiP target. A replica of the SHiP target with the same configuration was installed in the H4 beamline at the CERN SPS [54], [55].

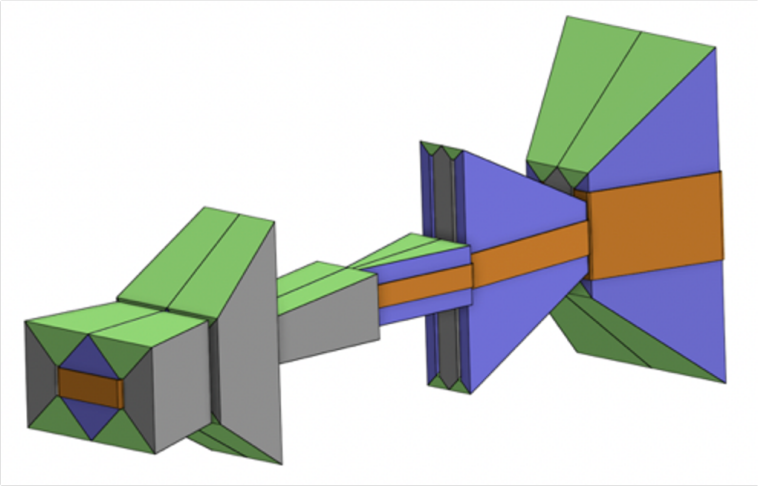

Figure 3.6: Schematic of muon shielding

The HS Spectrometer will allow the probing of any SM coupled new physics model with light long-lived exotic particles and masses below $\mathcal{O}(10)$ GeV/c^2. The detector is designed to fully reconstruct the exclusive decays of hidden particles occurring in the vacuum vessel and reject the background down to below 0.1 events in the sample

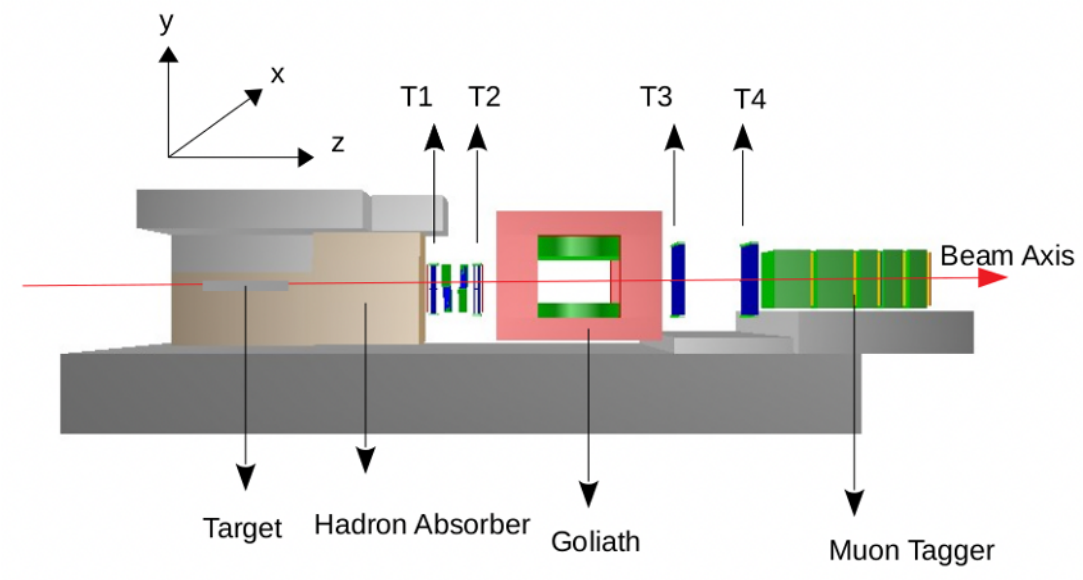

Figure 3.7: Layout of the muon flux test beam at 2018

of 2×10^{20} protons on target. The magnetic spectrometer is designed to accurately reconstruct the decaying particle's decay vertex, mass, and impact parameter at the target. In the case of conjunctive decay products, the timing detector allows the rejection of combinatorial backgrounds with $\sim$100 ps resolution. In the analysis, several selection criterion (Table 4.3 and 5.1) were used for the background rejection [56]. The electromagnetic calorimeter, SplitCal, is designed to provide electron identification and π^0 reconstruction. It has requirements to include reconstruction of ALP decaying to the two-photon that is the unique way to discriminate between an ALP and a DP (see Table 3.2). SplitCal also improves the electron/hadron separation. This allows SHiP not to use hadronic calorimeter without compromising the PID performance and only leave the absorber for muon filtering.

Table 3.2: Decay modes of DP and ALP that can be reconstructed at SplitCal

Particle	Final states
Dark Photon	$\ell^{\pm}\ell^{\mp}, h^{+}h^{-}$
ALP	$\gamma\gamma$

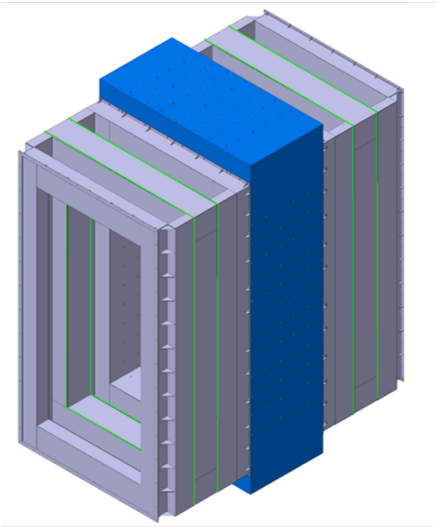

Figure 3.8: HS Spectrometer

A crucial component of the SHiP detector for the DP searches is HS Spectrometer Tracker(shown in Figure 3.8) since it reconstructs the charged particles produced by the decay of dark photons. Four tracking stations (T1 to T4) surround the dipole magnet with a field integral of $\sim$ 0.5 Tm, whereby T1 and T2 are on one side of the magnet and T3 and T4 on the other side; the set-up is schematically shown in Figure 3.9. A fifth station is located downstream of the vacuum vessel entrance lid. Each station consists of 9072 straw tubes arranged in four views (Y-U-V-Y), as shown in Figure 3.10. The Y view has straws horizontally aligned. The U and V views are subject to a θ_{stereo} = $\pm$ 5-degree rotation. The accuracy of the x coordinate measurements is therefore 1/sin(θ_{stereo}). This directly impacts the decay vertex measurements and the opening angle of the daughter particles (which enters the invariant mass), and the impact parameter at the production target. To provide a good spatial resolution and to minimize the contribution from multiple scattering, the straw tubes are made of thin polyethylene terephthalate (PET). More details about the Straw Detector's initial design can be found in [57]. The pattern recognition(PR) algorithms applied to the hits on the straw spectrometer are described in [58], and the algorithms for particle identification are presented in [56].

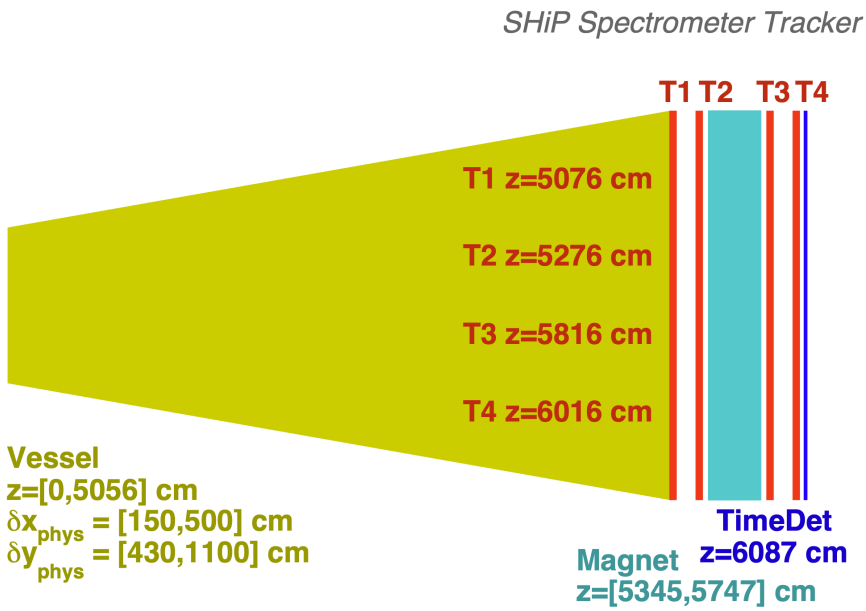

Figure 3.9: Positions of the tracking stations along the beam axis(z)

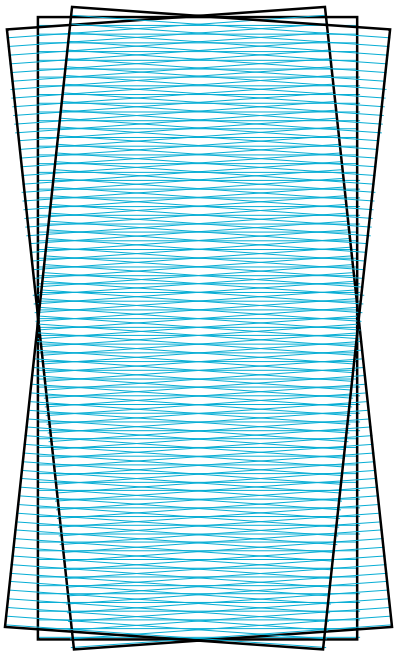

Figure 3.10: Schematic drawing of the three "views" that compose each straw chamber.

3.3 SHiP Software Framework

The software framework of the SHiP experiment, FAIRSHIP, is based on FairRoot [59]. It uses Pythia8.2 [60] for primary pp interactions, and Pythia6 [61] and GEANT4 [62] for inelastic interactions and heavy flavor production. GEANT4 is also responsible for the geometry of SHiP setup and interactions within the geometry. On the other hand, for the neutrino interactions, FAIRSHIP uses GENIE [63]. For the cascade productions, FAIRSHIP has two options; to produce the interactions only with GEANT4, or to produce the primary interactions from Pythia8, then the secondaries from GEANT4; these are explained in [64] and [65]. In the simulation of dark photons, a generator, *DPPythia8Generator*, is implemented. Dark photons are produced in the target from primary pp interactions by Pythia8.2, and their reconstructed charged decay products from HS Spectrometer, FITTRACKS, are considered. In the meantime, the cascades of secondary mesons are considered from Pythia8 and GEANT4 combination of FAIRSHIP.

CHAPTER 4

DARK PHOTON

In the vector portal's kinetic mixing model, the vector is an electrically neutral massive gauge boson called DP, which is the lightest particle of the new EM-like SM coupled force of the HS [27, 31, 66, 67]. DP is first mentioned in the investigation of the EM interactions below the defined mass scale of the elementary particle physics by introducing at least two very weakly interacting particles, called para-photons [68]. The theory is similar to QED, and the new vector particles have couplings to the EM. Furthermore, one of these new extra vector bosons has to be massless as photons. The kinetic mixing between para-photons and ordinary photons give rise to para-charged particles [69, 70]. In this way, the theory is defined as a vector portal model that connects the HS with SM. Nowadays, instead of para-photon, the name of DP is preferred. However, sometimes U-boson or HS-, heavy-, secluded- photons are used. The lagrangian of γ^{D} is given as

$$\mathcal{L} = \mathcal{L}_{\mathrm{SM}} - \frac{1}{4}\left(F'_{\mu\nu}\right)^2 - \frac{\varepsilon}{2}F'_{\mu\nu}F_Y^{\mu\nu} + \frac{1}{2}m^2_{\gamma\mathrm{D}}\left(A'_\mu\right)^2 \tag{4.1}$$

The field strength tensor, $F'_{\mu\nu} \equiv \partial_\mu A'_\nu - \partial_\nu A'_\mu$, of the $U(1)'$'s massive gauge field, A'_μ, whose vector gauge boson is γ^{D} . Kinetic mixing operator, ε, between $F'_{\mu\nu}$ and $F_Y^{\mu\nu}$, is dimensionless. $\varepsilon \sim 10^{-2}$ - 10^{-8} is generated through loops of particles charged under $U(1)_Y$ and $U(1)'$; the lower limit is evaluated from the case of one or both $U(1)$'s are contained in grand-unified-theory (GUT) groups, therefore, ε is only generated by two or three loop GUT-breaking effects. ε may contain a wide range of mixing. γ^{D} can have a mass, $\mathrm{m}_{\gamma^{\mathrm{D}}}$, if $U(1)'$ is broken by a Higgs-like mechanism. Thus, $\mathrm{m}_{\gamma^{\mathrm{D}}}$ could be obtained by the Stuckelberg mechanism, dark Higgs, or SM Higgs [17, 22, 28, 39, 44, 66, 67, 71, 72]. The equation of motion, $\partial_\mu F_{\mu\nu} = eJ_\nu^{\mathrm{EM}}$, would give

$$-\frac{\varepsilon}{2}F'_{\mu\nu}F_Y^{\mu\nu} \Rightarrow A'_\mu \times (e\varepsilon)J_\mu^{\mathrm{EM}} \tag{4.2}$$

Hence the coupling would be through EM current with a strength, reduced by a small factor ε. The interaction with the SM via EM current would conserve symmetries such as parity, flavor, and CP. It does not couple with neutrinos directly [17, 22, 31, 38, 39, 41, 44, 66, 67, 71–75]. As ε goes to zero, two sectors decouple. The lifetime of γ^{D} depends on $m_{\gamma^{\mathrm{D}}}$ and ε, and it is proportional to $(1/m_{\gamma^{\mathrm{D}}}\,\varepsilon^2)$.

In general, γ^{D} can explain the anomalous magnetic moment of the muon, cosmic ray dark matter anomalies such as positron to electron ratio and no excess of antiprotons, γ rays from electron-positron annihilation at the galactic center [22, 41, 42, 44, 76, 77].

Unfortunately, colliders and electron beam dumps have not been successful in providing a clue about γ^{D} until now [17, 28, 44, 77]. Meantime, analyses of all previous beam dump experiments give excluded limits on lower masses and smaller ε. The upper boundary is due to the short lifetime to reach the detector, and the lower boundary is due to the ε, which is too small to produce enough γ^{D} statistics.

The MC simulation for the direct detection sensitivity of SHiP to γ^{D} search consists of several steps:

- producing MC events with Pythia8. Each event is weighted; to produce γ^{D} at the target, to decay γ^{D} into the direct daughters at the vacuum vessel,

- simulating the SHiP detector response of the produced MC events through GEANT4,

- evaluating the limits at different ($m_{\gamma^{\mathrm{D}}}$, ε) points which scale logarithmically for ε and $m_{\gamma^{\mathrm{D}}}$ steps extends from 0.001 GeV to 1 GeV.

4.1 Dark Photon Production Mechanisms

The first step of MC simulation is to produce γ^{D} inside the target with a beam smear of $\pm$ 1 cm at each MC event by a weight factor (see Equation 6.2) that considers its production rate at the target, and decay rate at the vacuum vessel. Later, MC events are normalized using the weight factor. The possible production modes of γ^{D} [17, 27, 39, 42, 44, 73]:

- Light mesons decays
- Proton-bremsstrahlung
- Drell-Yan production

The Feynman diagrams of these production mechanisms are shown in Figure 4.1. Each production mechanism is discussed in the following sections.

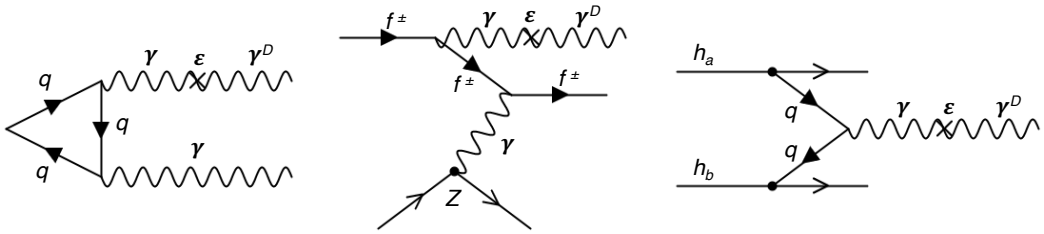

Figure 4.1: γ^{D} production modes: secondary meson production, proton-bremsstrahlung production, Drell-Yan (QCD) production

4.1.1 Secondary Meson Decays

Proton beam dumped experiments with heavy fixed-targets are suitable to search for γ^{D} in the decays of light pseudoscalar meson and light vector meson. Since then, the mass range goes up to $\sim$ 1 GeV. Beyond this mass, BR to ordinary photon decay modes negligible.

The grid points of the production are selected in the range of m_{γ^D} = (0.002 GeV, 0.90 GeV) and ε = (10^{-2}, 10^{-8}). The secondary mesons are produced by an interaction of the proton beam with the energy of 400 GeV to a proton in the target (similar result found on fixed neutron with the Molybdenum p:n ratio). Since the diffractive process does not contribute significance for meson products, Pythia8.2 is set to non-diffractive processes, *SoftQCD:nonDiffractive = on*, for inclusive QCD production. Then, BR of the production modes to γ^D is calculated from

$$\mathrm{BR}(\mathcal{P} \to \gamma^D \gamma) \simeq 2\varepsilon^2 \left(1 - \frac{m^2_{\gamma^D}}{m^2_{\mathcal{P}}}\right)^3 \mathrm{BR}(\mathcal{P} \to \gamma\gamma) \tag{4.3}$$

where pseudoscalar mesons, $\mathcal{P}$, are π^0, η and η'.

$$\begin{aligned}\mathrm{BR}(\mathcal{V} \to \mathcal{P}\gamma^D) \simeq{}& \varepsilon^2 \times \mathrm{BR}(\mathcal{V} \to \mathcal{P}\gamma) \\ &\times \frac{[(m^2_{\gamma^D} - (m_{\mathcal{V}} + m_{\mathcal{P}})^2)(m^2_{\gamma^D} - (m_{\mathcal{V}} - m_{\mathcal{P}})^2)]^{3/2}}{(m^2_{\mathcal{V}} - m^2_{\mathcal{P}})^3}\end{aligned} \tag{4.4}$$

where vector meson $\mathcal{V}$ is ω with pseudoscalar meson daughter ($\mathcal{P}$), π^0.
Those modes are originally taken from PDG [79] by replacing one of the decay product with γ^D (see Table 4.1).

Table 4.1: Branching ratios of γ modes, and the γ replaced by γ^D

m_{γ^D}(GeV)	production mode	BR	n_{meson} per pp
$0 - 0.135$	$\pi^0 \to \gamma^D\gamma$	0.98799	6.147 ± 0.003
$0 - 0.548$	$\eta \to \gamma^D\gamma$	0.3931181	0.703 ± 0.008
$0 - 0.648$	$\omega \to \gamma^D\pi^0$	0.0834941	0.825 ± 0.009
$0 - 0.958$	$\eta' \to \gamma^D\gamma$	0.0219297	0.079 ± 0.003

Since the MC production completely relies on Pythia8 in this mode, kinematics of mediator mesons must be investigated. In order to do that, Feynman X_F variable of the mesons are computed as a function of $P_Z/(P_p \times \theta)$, where P_Z is meson's momentum in Z-direction, θ is the meson's opening angle, and P_p is the momentum of

the proton beam and it is restricted in the region of $0.025 < X_F < 0.3$. Then, the differential-cross-sections as a function P_T and rapidity are evaluated in the parameter space of interest. The results of the comparisons are found similar to [35, 75] (see Figure 4.2).

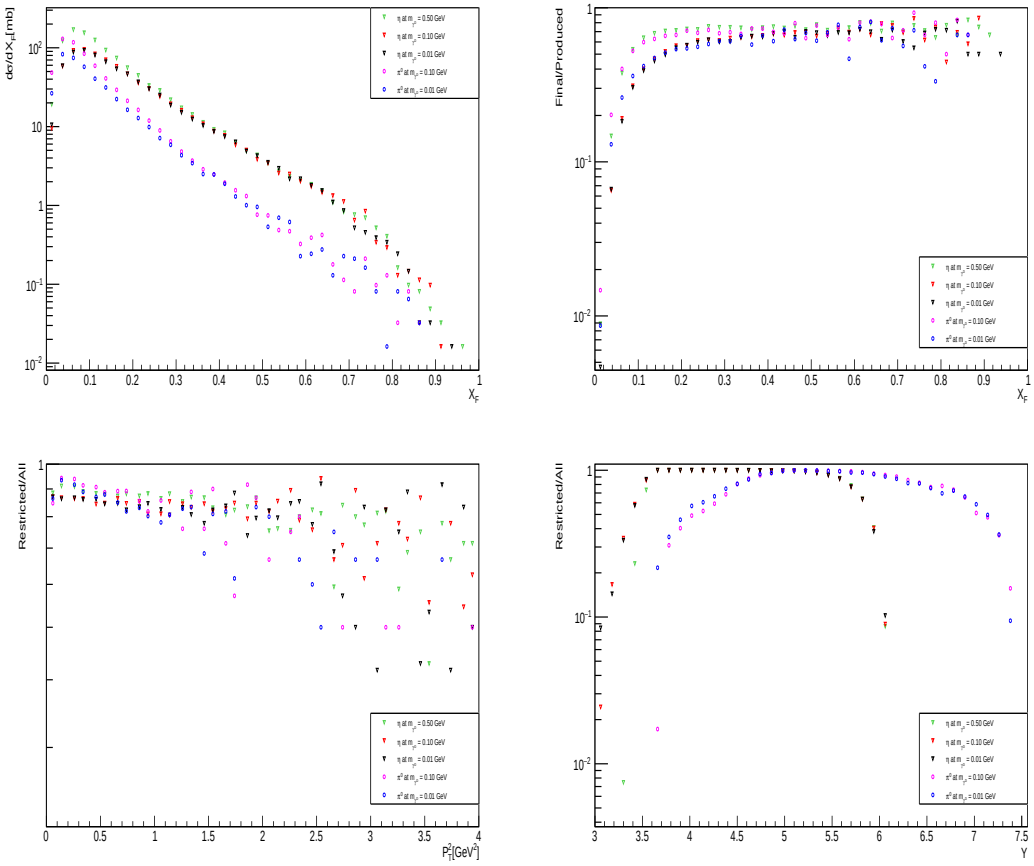

Figure 4.2: Kinematics of mediator mesons from Pythia8. Top left; X_F versus dσ with respect to X_F, top right; ratio of final events to all events as a function of X_F, bottom left; restricted region ($0.025 < X_F < 0.3$) to all region ratio as a function of P_T^2, and bottom right; restricted region to all ratio as a function of rapidity. π^0 and η are considered.

The γ^{D} production cross-section from the secondary meson decays, σ_{meson}, is evalu-

ated through

$$\sigma_{\text{meson}} = \sigma^{\text{inelastic}}_{\text{SHiP}} \times \sum_{\text{mesons}} \Theta\left(m_{\text{meson}} - m_{\gamma^{\text{D}}}\right) \times n_{\text{meson per pp}} \times \text{BR}\left(\text{meson} \rightarrow \gamma^{\text{D}} + X\right) \tag{4.5}$$

As it can be seen from Equations 4.3, 4.4, the production cross-section is suppressed by ε^2 since the main decay is EM.

4.1.2 Proton Bremsstrahlung

Quasielastic scattering of incident protons on nucleons in the target can produce γ^{D} via bremsstrahlung process $pp \rightarrow pp\ \gamma^{\text{D}}$, which is known as proton-bremstrahhlung (pbrem). It is very similar to the production of vectors via electron collision with nuclei (e-brem). Nevertheless, e-brem is tested well enough in the previous experiments, and even more it is studied in the SHiP setup in the [21], and the results are found negligible compare to the other production mechanisms. The mass range goes up to ~ 3 GeV while ε is between 10^{-3} and 10^{-9}. The approach of Fermi-Williams-Weizsacker is used to calculate production rates of pbrem [27, 67, 74, 80].

$$\begin{aligned} \frac{d^2N}{dzdp_\perp^2} &= \frac{\sigma_{pp}(s')}{\sigma_{pp}(s)}\, w_{ba}(z, p_\perp^2)\,, \\ w_{ba}(z, p_\perp^2) &= \frac{\varepsilon^2 \alpha_{\text{QED}}}{2\pi H}\left[\frac{1+(1-z)^2}{z} - 2z(1-z)\left(\frac{2m_p^2 + m_{\gamma^{\text{D}}}^2}{H} - z^2\frac{2m_p^4}{H^2}\right)\right. \\ &\quad \left. +2z(1-z)\big(1+(1-z)^2\big)\frac{m_p^2 m_{\gamma^{\text{D}}}^2}{H^2} + 2z(1-z)^2\frac{m_{\gamma^{\text{D}}}^4}{H^2}\right], \end{aligned} \tag{4.6}$$

where $\sigma_{pp}(s)$ ($\sigma_{pp}(s')$) are the total pp cross-sections for the incoming (outgoing) proton energies. m_p, P and E_p are the proton beam's mass([79]), its initial momentum and its energy, respectively. p and $E_{\gamma^{\text{D}}}$ are the momentum and energy of the γ^{D} . $p_\perp$ and $p_\parallel$ are the components of the γ^{D} momentum. z is the fraction of the proton momentum that is carried away by γ^{D} in the beam direction, and α_{QED} is the QED fine structure constant, which is 1/137. $s' = 2m_p(E_p - E_{\gamma^{\text{D}}})$, $s = 2m_pE_p$ and $H(p_\perp^2, z) = p_\perp^2 + (1-z)m_{\gamma^{\text{D}}}^2 + z^2m_p^2$ [21, 27, 67, 74]. The nuclear effects of bounded protons cancel the ratio of $\frac{\sigma_{pp}(s')}{\sigma_{pp}(s)}$ [27]. However, this calculation does not

consider the QCD contributions when m_{γ^D} is above the proton mass. In that situation, the possible contributions to the cross-section from the nuclear resonances of the vector mesons, named as Vector Meson Dominance(VDM) [74,81,82], is considered.

Thus, two independent scenarios are studied in [27]. When m_{γ^D} is heavier than 1 GeV, dipole form factor (FF) [83] considers a penalty factor for the strong suppression of the production:

$$\text{penalty}(m_{\gamma^D}) = \left(\frac{m^2_{\gamma^D}}{0.71\,\text{GeV}^2} \right)^{-4} \quad \text{for} \quad m^2_{\gamma^D} > 0.71\,\text{GeV}^2\,. \tag{4.7}$$

Then, the penalty dipole form factor, FF_{dipole}, is applied to Equation 4.6. However, [21] states that FF_{dipole} does not consider QCD contributions once m_{γ^D} is bigger than proton mass. This can be overcome by VMD, which gives contributions around the masses of ρ and ω. Then, it continues to give some contributions around the 1.25 GeV - 1.45 GeV [82]. VDM FF, FF_{VDM}, is applied into Equation 4.6.

The total p-p cross section $\sigma_{pp}(s)$ is given as

$$\sigma_{pp}(s) = Z + B \cdot \log^2\left(\frac{s}{s_0}\right) + Y_1 \left(\frac{s_1}{s}\right)^{\eta_1} - Y_2 \left(\frac{s_1}{s}\right)^{\eta_2}\,, \tag{4.8}$$

where $Z = 35.45$ mb, $B = 0.308$ mb, $Y_1 = 42.53$ mb, $Y_2 = 33.34$ mb, $\sqrt{s_0} = 5.38$ GeV, $\sqrt{s_1} = 1$ GeV, $\eta_1 = 0.458$ and $\eta_2 = 0.545$ [84]. Equation 4.6 is extracted as a function of the γ^D angle θ and its momentum, p:

$$\begin{aligned} P_p^\mu &= \left(E_p, P_p, \overrightarrow{P}_{p\perp} = \overrightarrow{0}\right) \\ p^\mu &= \left(E\left(z, P_p, \theta\right), zP_p, \overrightarrow{p}_\perp(\theta)\right) \\ \text{where } \theta = p_\perp / zP_p \text{ and } p &= \sqrt{p_\perp^2 + z^2 P_p^2} = \sqrt{z^2 P_p^2\left(\theta^2 + 1\right)} \end{aligned}$$

It follows as

$$\frac{dN}{dpd\theta} = \frac{dN}{dzdp_\perp^2}\frac{dP_\perp^2}{d\theta}\frac{dz}{dp}$$
$$\frac{dp_\perp^2}{d\theta} = 2p_\perp\frac{dp_\perp}{d\theta} = 2p_\perp zP_p = 2\theta z^2 P_p^2$$
$$\frac{dp}{dz} = \frac{zP_p^2\left(\theta^2+1\right)}{\sqrt{z^2P_p^2\left(\theta^2+1\right)}} = P_p\sqrt{\theta^2+1} \Rightarrow \frac{dz}{dp} = \frac{1}{P_p\sqrt{\theta^2+1}}$$

Then, $f(p,\theta)$ is

$$\frac{dN}{dpd\theta} = \frac{\sigma_{pp}(s')}{\sigma_{pp}(s)}w_{ba}(z,p_\perp^2)\frac{2\theta z^2 P_p}{\sqrt{\theta^2+1}} \tag{4.9}$$

It is worth to emphasize that the normalized PDF is independent of ε. From Equation 4.9, a two-dimensional normalised probability density function(PDF), $f(p,\theta)$, is plotted in Figure 4.3 for two different m_{γ^D} values.

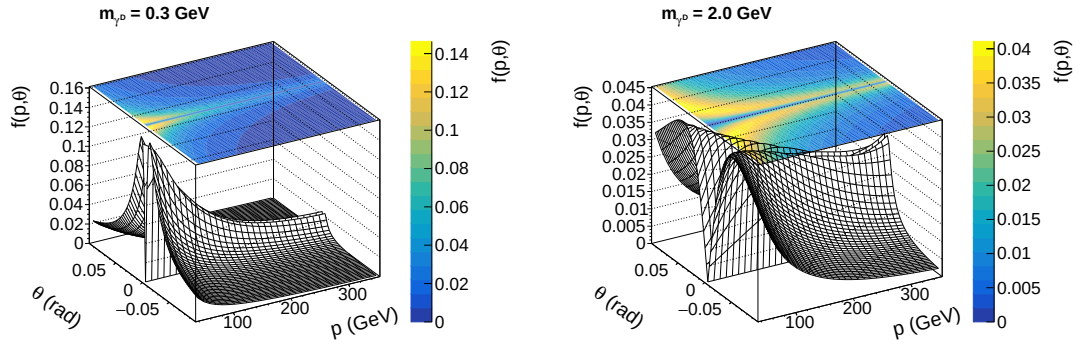

Figure 4.3: 2D normalized PDF as a function of θ and p for two different choices of m_{γ^D} : 0.3 GeV on left, and 2 GeV on right. This plot is taken from [27].

Finally, the cross-sections of the two method of Dipole FF and VDM FF, are given as:

$$\sigma_{\text{pbrem}} = \sigma_{\text{SHiP}}^{\text{inel}} \times \int_{p_{\min}}^{p_{\max}}\int_{\theta=-\theta_{\max}}^{\theta_{\max}} \text{FF}_{\text{Dipole or VDM}} \times \frac{d^2N}{dpd\theta}\,d\theta dp\,, \tag{4.10}$$

The bounds of p in Equation 4.10 are $0.1\times P_{\text{p}}$ [74], and $0.9\times P_{\text{p}}$. Meantime, $p_\perp < 4$ GeV gives $\theta_{\max} \simeq 0.1$ rad.

Then, the production is performed in the range of m_{γ^D} = (0.002 GeV, 3.50 GeV) and ε = (10^{-3}, 10^{-9}). For each (m_{γ^D} ,ε) point, γ^D kinematics are assigned by the randomly chosen (p, θ) points from Figure 4.3 in each MC event.

4.1.3 Drell-Yan

In the Drell-Yan process, instead of producing a virtual photon or Z-boson, γ^D is produced through the annihilation of a quark and an antiquark from different hadrons. The process is like $q + \bar{q} \rightarrow \gamma^D \rightarrow q + g \rightarrow q\gamma^D$. The signal of γ^D can provide decay vertex and invariant mass measurement, unlike the other two mechanisms [85, 86]. The Pythia8 class of HiddenValley [87] was used between grid points m_{γ^D} = (1.5GeV,10.0GeV) and ε =(10^{-2},10^{-8}). The lower limit of m_{γ^D} , 1.4 GeV, is found due to the lack of perturbative QCD domain [27]. The extraction of the empirical cross-section of the Drell-Yan γ^D production is performed in [27]:

$$\begin{aligned} 1.4 < m_{\gamma^D} \leq 3\text{GeV} : \sigma_{\text{QCD}} &= \varepsilon^2 \times e^{-2.05488-1.96804\times m_{\gamma^D}} \\ m_{\gamma^D} > 3\text{GeV} : \sigma_{\text{QCD}} &= \varepsilon^2 \times e^{-5.51532-0.830917\times m_{\gamma^D}} \end{aligned} \tag{4.11}$$

In all three productions, the cross-sections are proportional to ε^2, and comparison of each production cross-section is shown in Figure 4.4.

4.2 Decay Channels

Giving the fact that γ^D has mixing with ordinary photon through loops of particles charged under $U(1)'$ and $U(1)'_Y$, and assuming the lightest HS particle assumption make them allow to decay into $\ell^+ \ \ell^-$ and $q \ \bar{q}$. The resulting decay widths, Γ, for lepton and hadrons (invisible decay mode is neglected in this model), are

$$\Gamma(\gamma^D \rightarrow \ell^+\ell^-) = \frac{1}{3}\alpha_{QED} m_{\gamma^D} \varepsilon^2 \sqrt{1 - \frac{4m_\ell^2}{m_{\gamma^D}^2}} \left(1 + \frac{2m_\ell^2}{m_{\gamma^D}^2}\right) \tag{4.12}$$

where m_ℓ is the mass of the lepton mode, and $\alpha_{\text{QED}} = \frac{1}{137}$

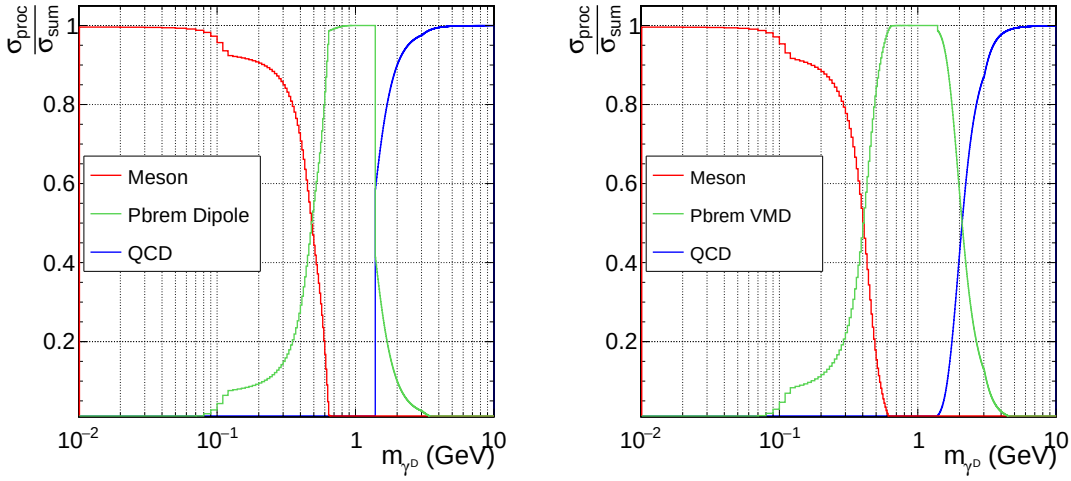

Figure 4.4: The cross-sections as a function of m_{γ^D} for each production mechanisms; meson(red), pbrem dipole(green on left), pbrem VDM(green on right), and Drell-Yan(blue). This plot is taken from [27].

$$\Gamma(\gamma^{\mathrm{D}} \rightarrow \text{ hadrons}) = \Gamma(\gamma^{\mathrm{D}} \rightarrow \mu^+\mu^-) R\left(m_{\gamma^{\mathrm{D}}}\right) \tag{4.13}$$

where

$$R\left(\sqrt{s}\right) = \frac{\sigma(e^+e^- \rightarrow hadrons)}{\sigma(e^+e^- \rightarrow \mu^+\mu^-)} \tag{4.14}$$

$$\tag{4.15}$$

With the fact that R-ratio is unitless; Equation 4.13 is defined from the cross-section of the electron pair annihilation into hadrons [90] by using the decay width of the γ^{D} instead of the cross-sections of the electron. Finally, from the energy-time uncertainty relation, the lifetime (τ) is inverse of the total width:

$$\tau = \frac{\hbar}{\Gamma_{\text{total}}} \tag{4.16}$$

Hence, the lifetime of γ^{D} is inversly proportional to ε^2. The last ingrendient of the analysis, the branching ratio to the modes is

$$\mathrm{BR}_{\mathrm{mode}} = \frac{\Gamma_{\mathrm{mode}}}{\Gamma_{\mathrm{total}}} \tag{4.17}$$

Then, branching ratio is independent of ε.

In the MC production, the decay of γ^{D} is handled by Pythia8, and the branching ratios to the kinematically allowed decay modes are defined from Equations 4.12, 4.13. Nevertheless, Equation 4.13 considers the whole hadronic modes as one channel. Then, the sum of the branching ratios of the each individual pair is equal to the total hadronic branching ratio, $\mathrm{BR}_{\mathrm{hadron}}$:

$$\mathrm{BR}_{\mathrm{hadron}}(\mathrm{m}_{\gamma^D}, \varepsilon) = \sum_{\mathrm{quarks}} \mathrm{BR}_{q_i\bar{q}_i}(\mathrm{m}_{\gamma^D}, \varepsilon)$$

Since γ^{D} does coupling to the $q\bar{q}$ pairs through the EM current, BR of each $q\bar{q}$ pair is proportional to their EM charge (Q) [91]:

$$\mathrm{BR}_{q\bar{q}}(\mathrm{m}_{\gamma^D}, \varepsilon) = \mathrm{BR}_{\mathrm{hadron}}(\mathrm{m}_{\gamma^D}, \varepsilon) \times \frac{Q_q^2}{\sum_{\mathrm{quarks}} \Theta(\mathrm{m}_{\gamma^{\mathrm{D}}} - m_{q_i})\, Q_{q_i}^2} \tag{4.18}$$

where the step function Θ ensures γ^{D} decay into the pair to obey the kinematical condition.

Each ($\mathrm{m}_{\gamma^{\mathrm{D}}}$, ε) point gives different decay-width, hence, different lifetime. The direct products of γ^{D} are boosted in Z direction to be inside the vessel from the weight, $\mathrm{w}_{\mathrm{vtx}}(\ell)$ (see Equation 6.2):

$$\lambda = \frac{\ell}{P} \tag{4.19}$$

$$V_{x,y,z}^{boosted} = V_{x,y,z} + \lambda \times P_{x,y,z} \tag{4.20}$$

As it was stated, the algorithm of DP production differs in each production mechanism. However, we will see that the kinematics of the productions would be similar since they were interpreted from the same decay formulas.

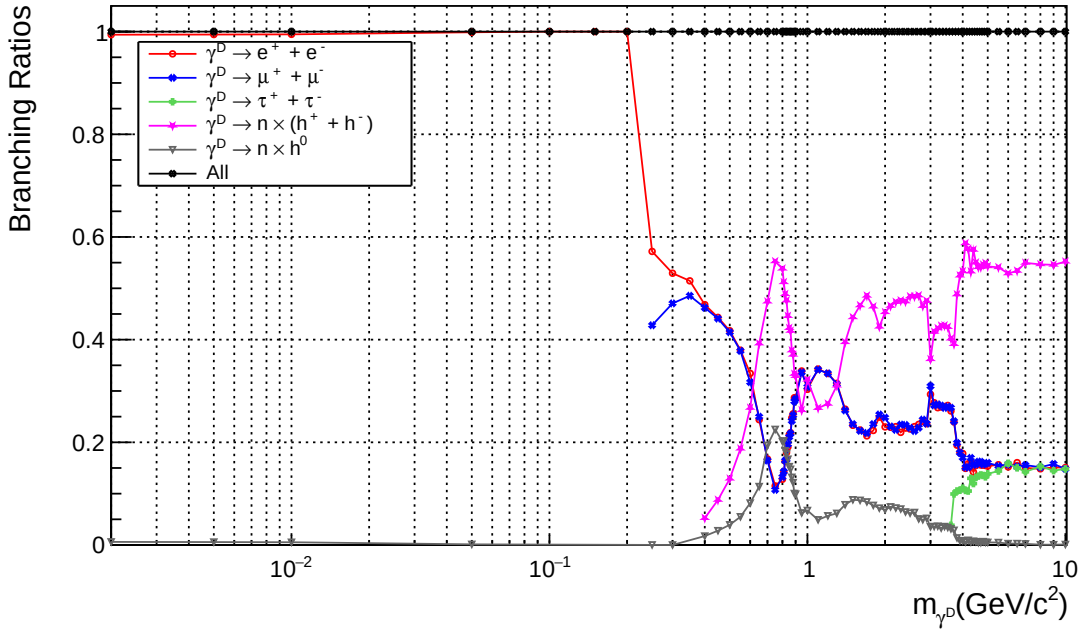

Figure 4.5: γ^D BR as a function of m_{γ^D}

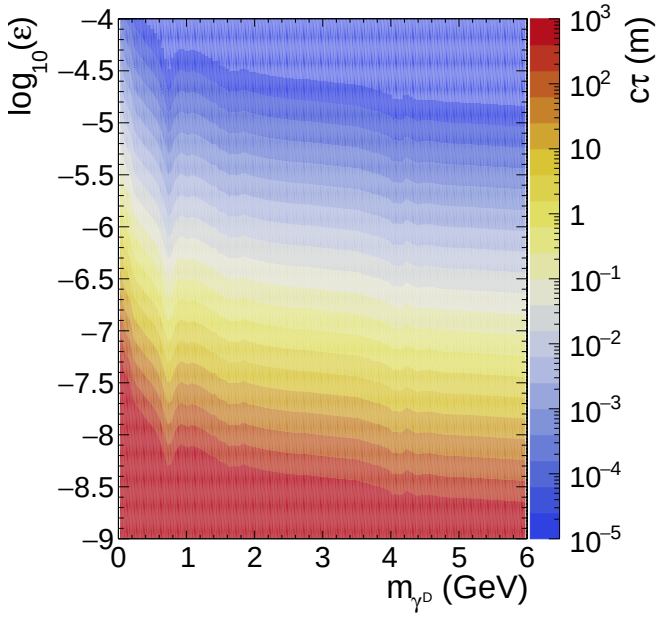

Figure 4.6: Lifetime of γ^D as a function of m_{γ^D} and ε. This plot is taken from [27].

Finally, MC events of γ^D and direct daughters are passed through GEANT4 to simulate the SHiP detector's response. Once the MC events with detector response are produced, the final charged stable products of γ^D are reconstructed by the FairShip reconstruction algorithm [56, 58].

Table 4.2: Decay Channels kinematically allowed and visible channels

Decay type	Decay mode	Final State visibility at the reco level
Leptons	$\gamma^{\mathrm{D}} \to e^- + e^+$	visible
	$\gamma^{\mathrm{D}} \to \mu^- + \mu^+$	visible
	$\gamma^{\mathrm{D}} \to \tau^- + \tau^+$	visible
Charged hadrons	$\gamma^{\mathrm{D}} \to \mathrm{n} \times (h^- + h^+)$	visible
	$\gamma^{\mathrm{D}} \to \mathrm{n}_1 \times (h^- + h^+) + \mathrm{n}_2 \times h^0$	visible
Neutral hadrons	$\gamma^{\mathrm{D}} \to \mathrm{n} \times h^0$	invisible

4.3 Analysis

In order to estimate SHiP sensitivity, about 10k discrete grid points in ($\mathrm{m}_{\gamma^{\mathrm{D}}}$, ε) are produced and reconstructed to scan the interested phase-space of ε and $\mathrm{m}_{\gamma^{\mathrm{D}}}$.

The following selection criteria are applied for the event selection:

1. Purification criteria: at least two final stable charged products that were originated from γ^{D} decay,
2. Decay selection: decay occurs inside the vessel,
3. Criterias of Tracking stations and final selections: if they reconstructed in the Tracking Stations that passed through the HS Magnet with the hit in each stations, and selected as high quality tracks while estimating the background [56].

This procedure is detailed in Table 4.3.

Once all the requirements are satisfied, geometric acceptance, $\mathcal{A}_{\mathrm{geo}}$, is defined as

$$\mathcal{A}_{\mathrm{geo}} = \mathcal{P}_{\mathrm{vessel}} \times \mathcal{P}_{\mathrm{reco}} \tag{4.21}$$

$$\text{where } \mathcal{P}_{\mathrm{vessel}} = \frac{n_{vessel}^{w_{vtx}}}{n_{purified}} \text{ , } \mathcal{P}_{\mathrm{reco}} = \frac{n_{reco}^{w_{vtx}}}{n_{vessel}^{w_{vtx}}}. \tag{4.22}$$

Table 4.3: γ^{D} selections

Purification (Fig 4.7)	at least two charged MC products from allowed channels
Decay Selection (Fig 4.8)	MC vertex of FITTRACKS considers; Z should be inside the vessel by 6 m away from the vessel entrance and before the vessel exit, XY should be at least 5 cm away from vessel inner walls
Passing Tracker Stations	at least two charged final products extrapolated to the field of SHiP Magnet while still valid for the decay selection from the FITTRACK vertex.
Final Selection (Fig 4.9)	NDF > 25, $\chi^2/\mathrm{NDF} < 5$, DOCA < 1 cm, IP $<0.1\mathrm{m}$, P $> 1\mathrm{GeV}$

The following cuts were applied to provide a background rejection for RECO tracks

- **DOCA:** the distance of closest approach between RECO track and the MC track,
- **IP:** the distance of closest approach between RECO track and the MC track,
- **P>1 GeV:** Momentum cut to the MC tracks is used to better particle-identification on the RECO tracks.

The following cuts were used to select high-quality RECO tracks:

- **NDF:** number of degrees of freedom refers to the number of fitted hits for the RECO track since we want to hit in every tracking stations after and before the magnet,
- $\boldsymbol{\chi^2/\mathrm{NDF}}$**:** the χ^2 of the fitted hits is normalized by PDF to have a more reliable fit.

To summarize the behaviors of the each step:

- The $\mathcal{P}_{\text{purified}}$ equals to $\frac{n_{purified}}{n_{DP}}$, and it refers the visible channels BR that the detector is sensitive. The BR is shown in Figure 4.7. Only difference with the decay channels BR of γ^{D} is neutral hadronic decays (see in Table 4.2 and Figure 4.5), and the effect starts from the two π^0 masses.

- Vessel acceptance, $\mathcal{P}_{\text{vessel}}$, depends on the lifetime and kinematics of the γ^{D} . It goes up until the 5% to 10%

- The reconstruction efficiency, $\mathcal{P}_{\text{reco}}$, mostly over 80%. A dependency on ε is observed for the lower masses with lower epsilons in the meson production. This is related to the softer angular distributions of γ^{D} that leads to a ε dependency on the decay vertex in meson production.

- The geometric acceptance, $\mathcal{A}_{\text{geo}}$, is driven by $\mathcal{P}_{\text{vessel}}$ (see Figure 4.10).

- Furthermore, the uncertainties -blue color on unexpected areas- mainly caused by the low weights.

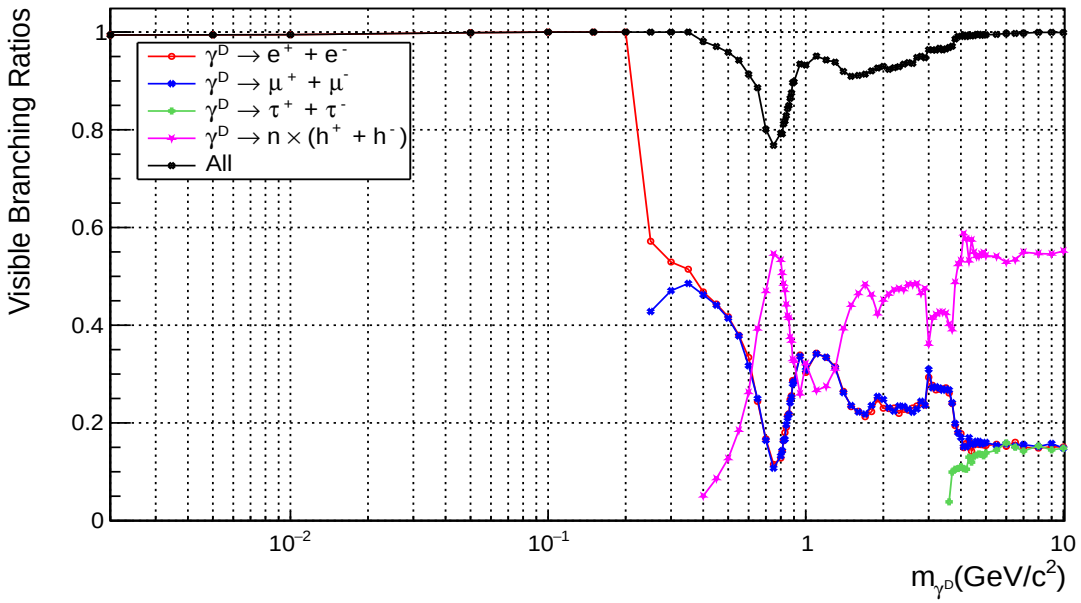

Figure 4.7: Visible Channel of γ^{D}

The kinematics of γ^{D} decay products are compared in three different masses and mechanisms before and after each selection in Figures 4.11, 4.12, 4.13 and Figures

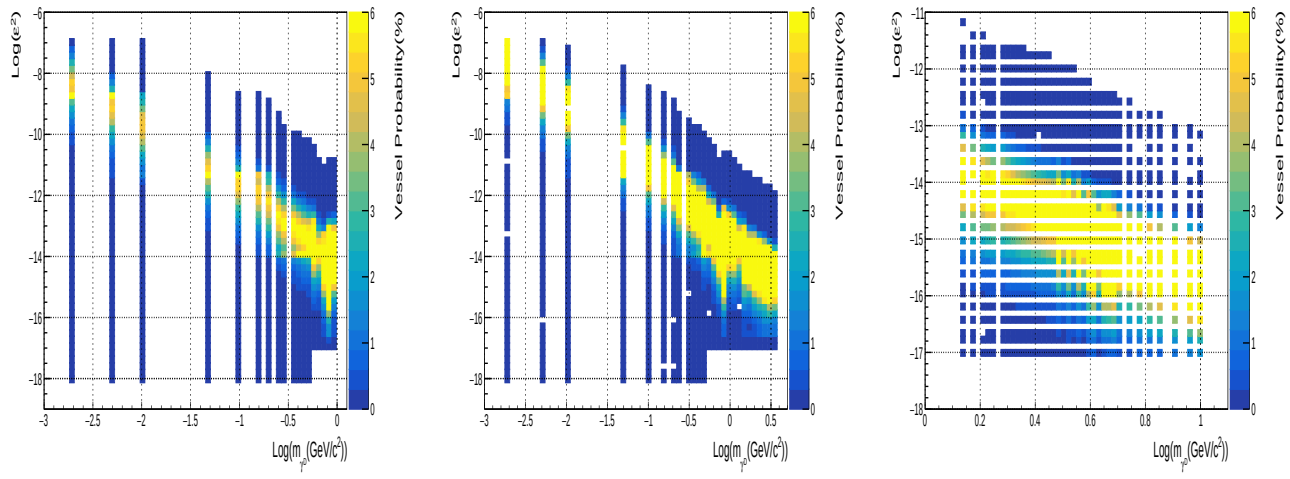

Figure 4.8: Vessel Probability of three different γ^{D} production mechanisms. From left to right: meson decays, pbrem, QCD.

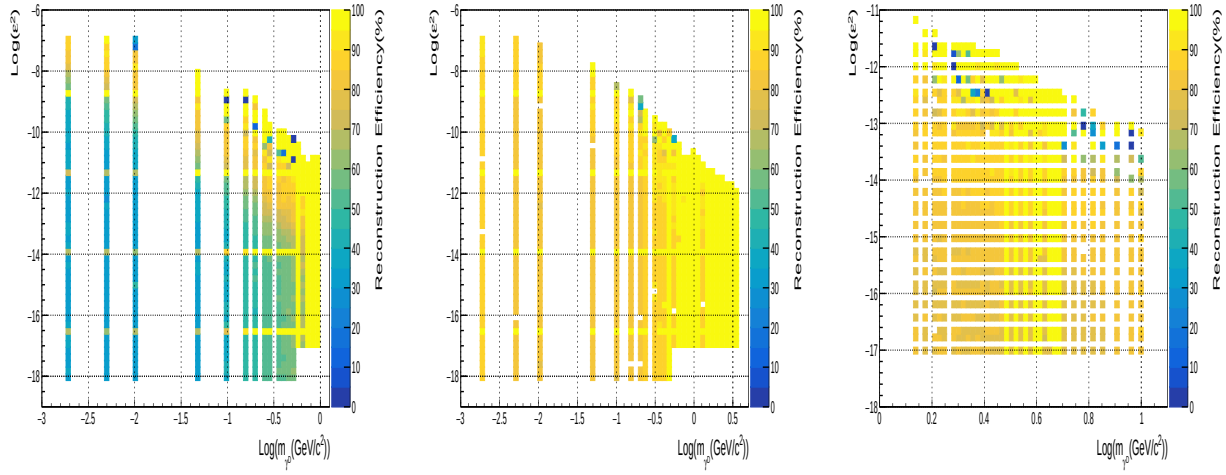

Figure 4.9: Reconstruction Efficiency of three different γ^{D} production mechanisms. From left to right: meson decays, pbrem, QCD.

4.14, 4.15, 4.16. Softer particles are discarded in the vessel selection.

4.3.1 Meson Cascade Factor

An additional study on the meson cascade enhancement factorization to the meson production modes are evaluated using the GEANT4 cascade and Pythia8 production.

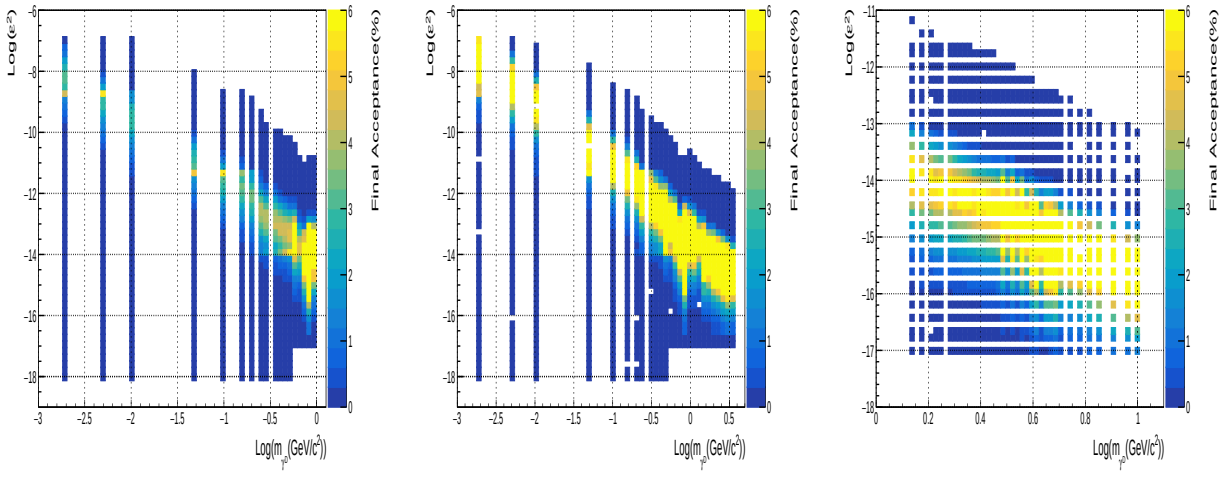

Figure 4.10: Geometric acceptance of three different γ^{D} production mechanisms. From left to right: meson decays, pbrem, QCD.

Since the enhancement cascade factor's systematic uncertainties are not estimated yet, the results are not considered as final results.

The cascade production is done in FAIRSHIP with the options of "E_{cut} = 0.5 GeV and Pythia8's *SoftQCD:nonDiffractive* = *on*". 1.5 M events are produced, and the multiplicities of primaries and secondaries were compared in Table 4.4. The Pz and rapidity distributions of each meson are divided and scaled by 1.5 M as shown in Figure 4.17.

Table 4.4: The average number of mediators from the cascades in pN collisions

mediator	Primaries from Pythia8	GEANT4 cascades with primary Pythia8
π^0	41.12	5.716
η	5.299	0.7018
ω	0.8757	0.824
η'	1.997	0.07886

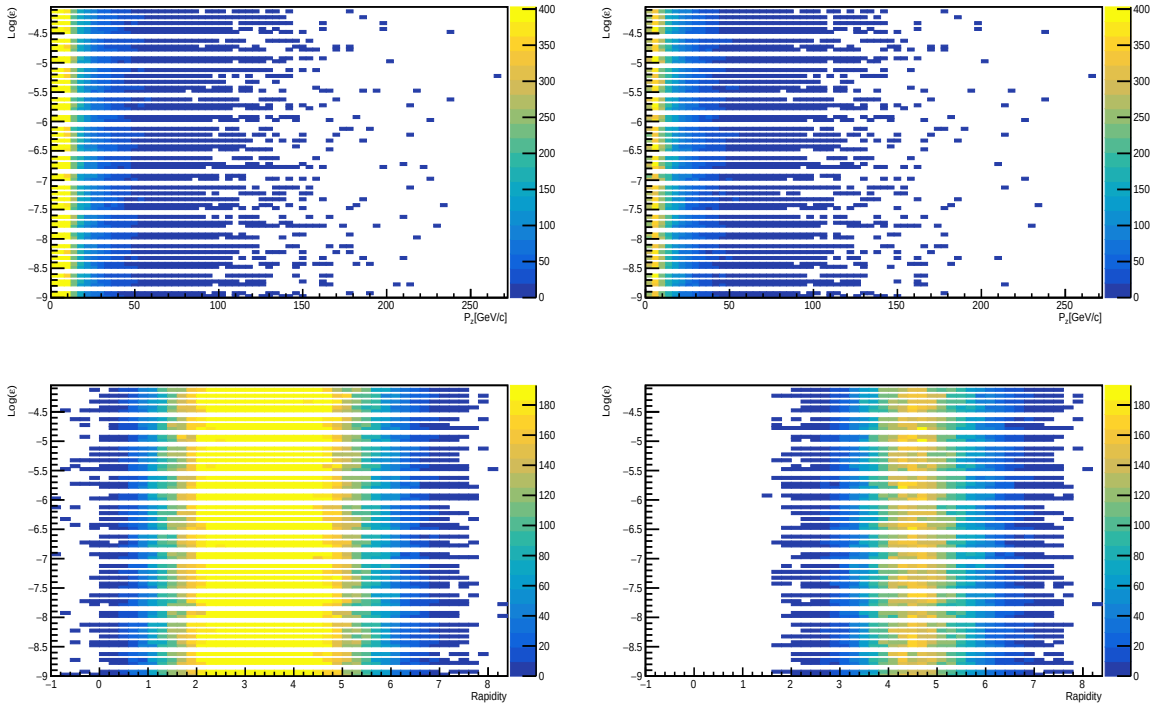

Figure 4.11: ε versus P_z and ε versus rapidity distributions of the decay products in the η production at the m_{γ_D} = 0.3 GeV. On left: the purified events. On right: the vessel selected events.

4.3.2 Estimation of Exclusion Contours

The geometric acceptance, $\mathcal{A}_{\text{geo}}$, and the production rate of the each mechanism, σ_{mode} (see Equations 4.5, 4.10, 4.11) are used to get the expected number of events, $\mathcal{N}_{\gamma_D}$(see Equation 6.1), at each (m_{γ_D} , ε) point. Then, the final step of the sensitivity analysis is to extract one lower ε limit and one upper ε limit for each m_{γ_D} point by interpolating the resultant $\mathcal{N}_{\gamma_D}$ to the limit of 2.3 events (2.3 event limit is discussed in detail at Chapter 6) with the class of ROOT::TEVAL. As an example, the extraction of the limits in three different masses are shown in Figure 4.18.

Besides having the limits for each production mode exclusively, two combined cases (meson and QCD with pbrem VDM and pbrem Dipole) are also considered. The systematic uncertainties are estimated as $\pm 30\%$ for mesons, $^{+50\%}_{-40\%}$ for pbrem, and $^{+10\%}_{-20\%}$ for Drell-Yan. The detailed explanation and estimation of the systematic uncertainties

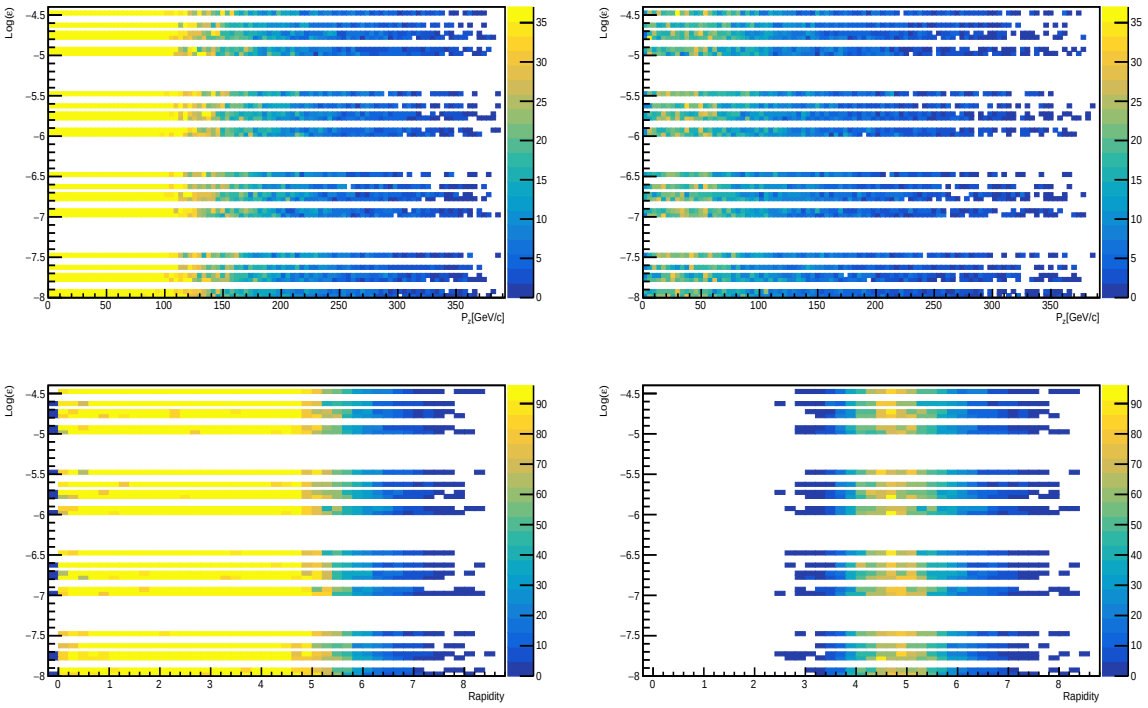

Figure 4.12: ε versus P_z and ε versus rapidity distributions of the decay products in the pbrem production at the m_{γ_D} = 1.0 GeV. On left: the purified events. On right: the vessel selected events.

are discussed in [27].

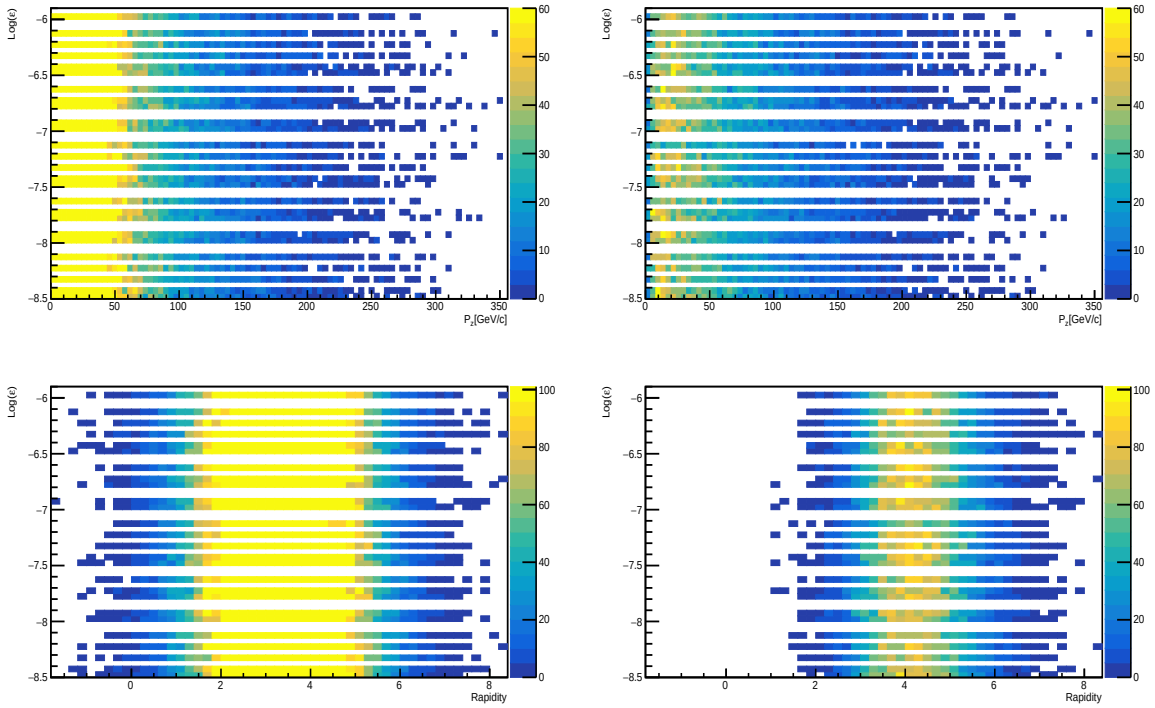

Figure 4.13: ε versus P_z and ε versus rapidity distributions of the decay products in the QCD(Drell-Yan) production at the m_{γ^D} = 3.0 GeV. On left: the purified events. On right: the vessel selected events.

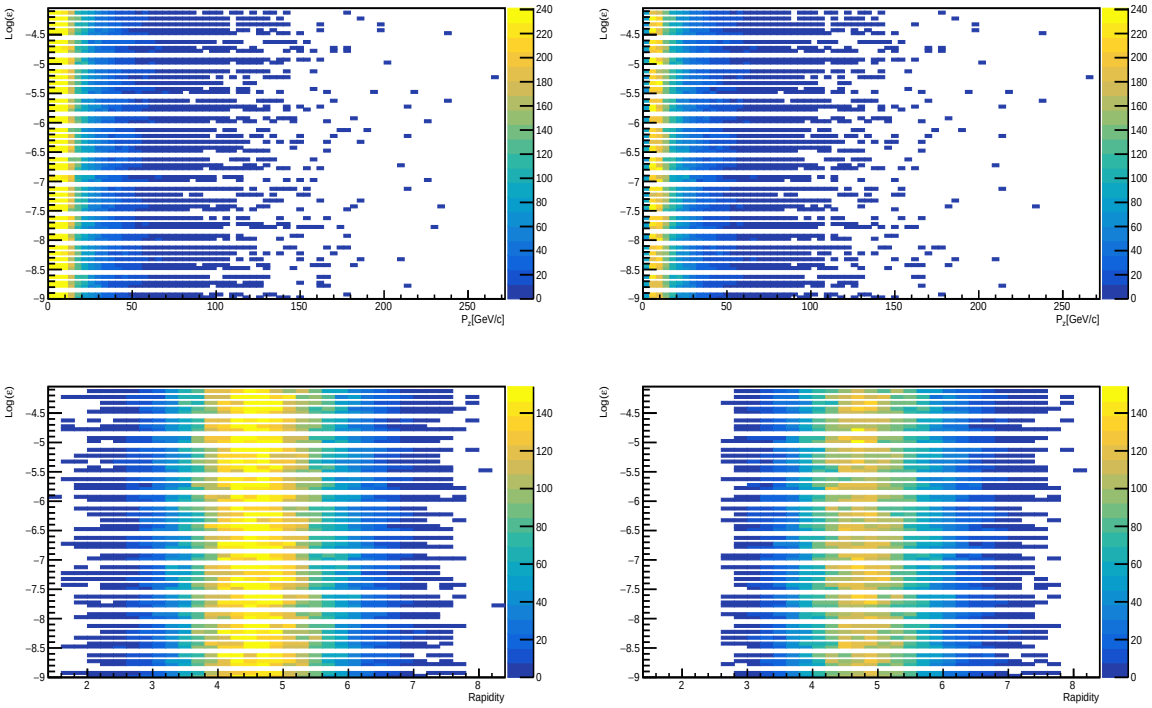

Figure 4.14: ε versus P_z and ε versus rapidity distributions of the decay products in the η production at the m_{γ^D} = 0.3 GeV. On left: the vessel selected events. On right: the final selected events.

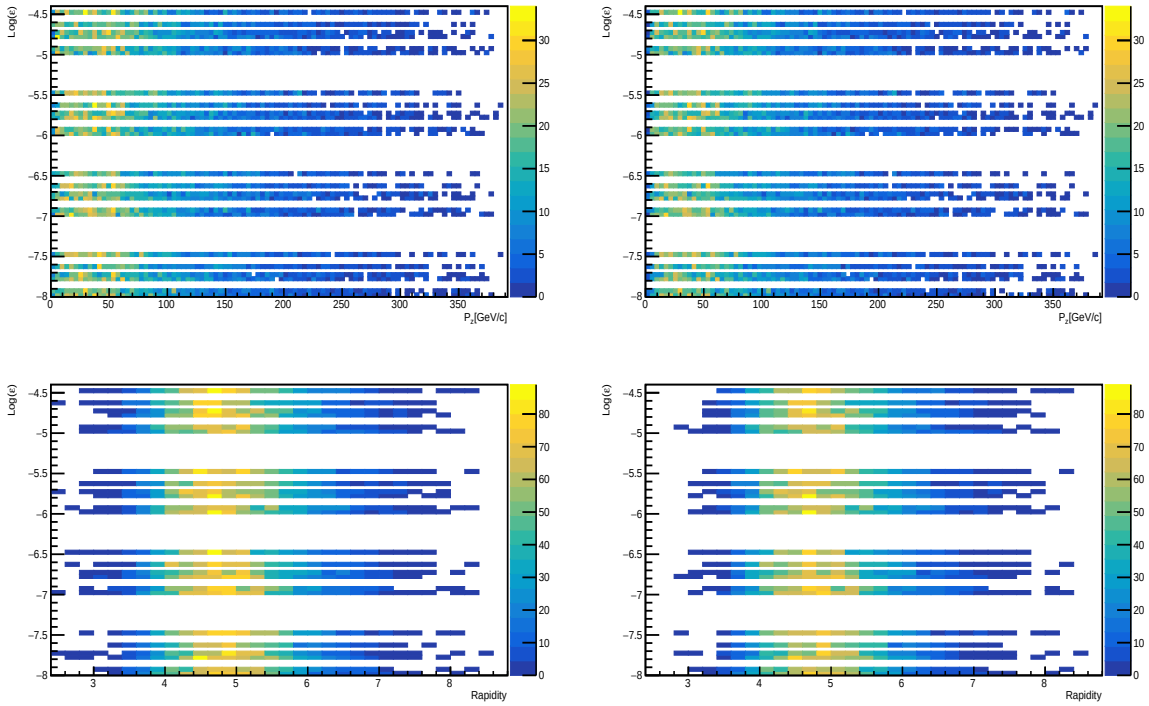

Figure 4.15: ε versus P_z and ε versus rapidity distributions of the decay products in the pbrem production at the m_{γ_D} = 1.0 GeV. On left: the vessel selected events. On right: the final selected events.

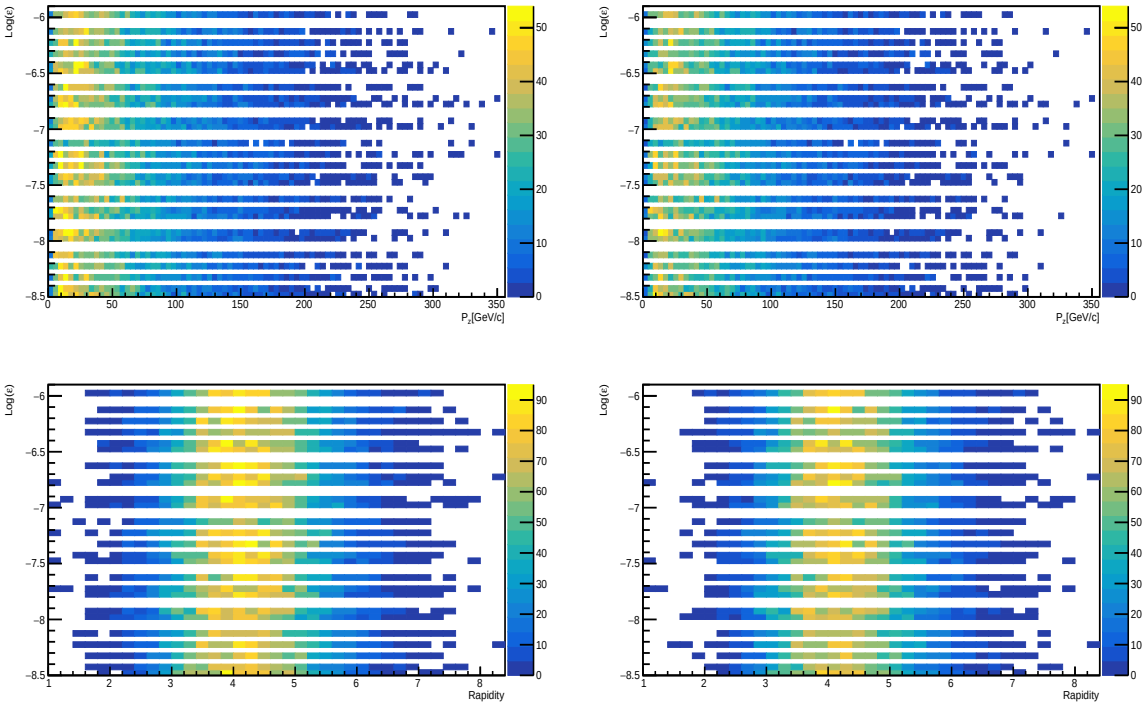

Figure 4.16: ε versus P_z and ε versus rapidity distributions of the decay products in the QCD(Drell-Yan) production at the m_{γ_D} = 3.0 GeV. On left: the vessel selected events. On right: the final selected events.

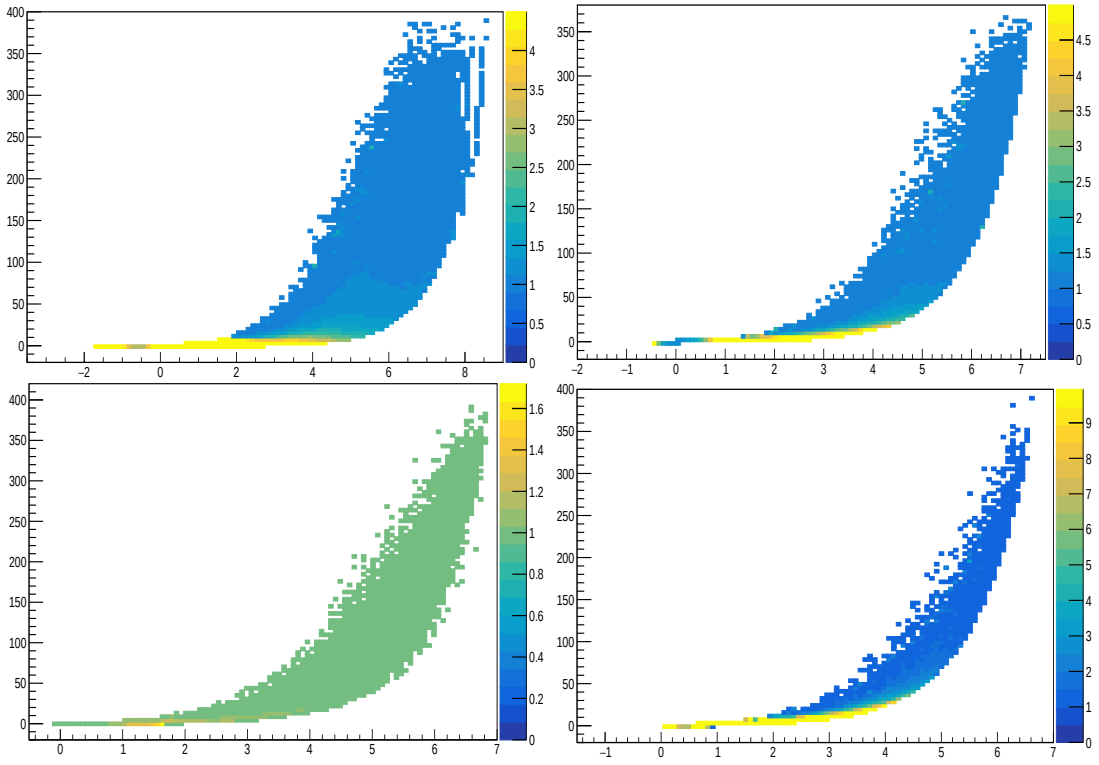

Figure 4.17: Cascade boost of π^0 (top left) , η (top right), ω (bottom left) and η' (bottom right).

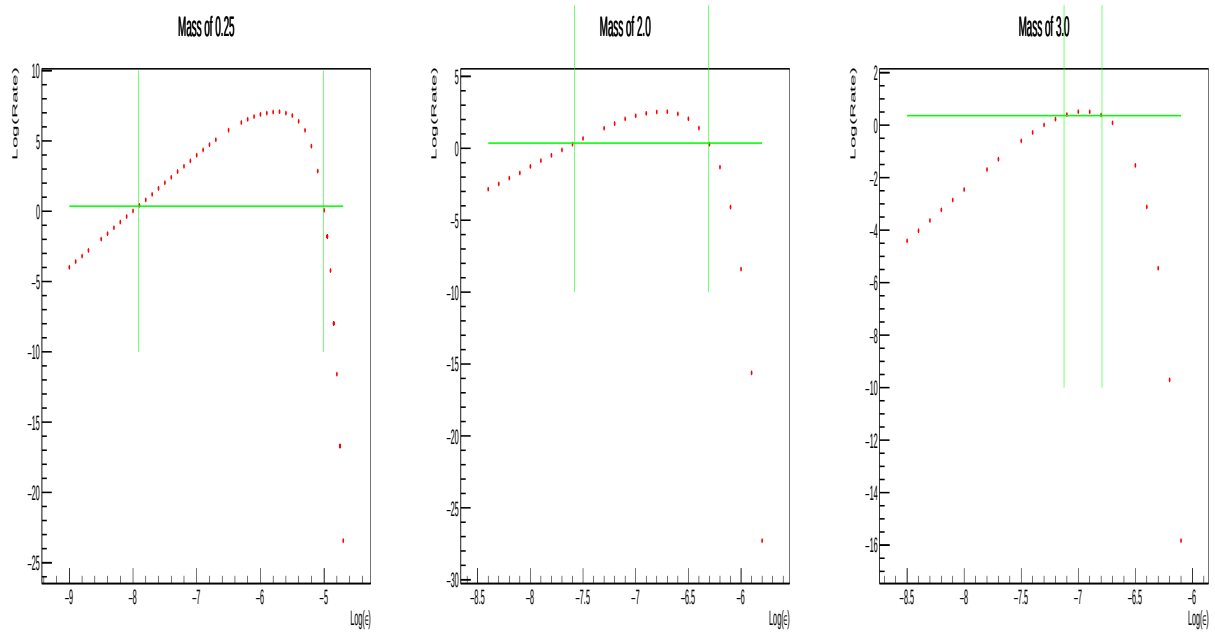

Figure 4.18: The lower and upper limits of ε (vertical green lines) for three different m_{γ_D} values.

CHAPTER 5

AXION LIKE PARTICLES

The existence of new elementary (light or pseudo)scalar, spin-0 bosons, is motivated by the Higgs boson discovery. The new particles can be light and interact very weakly with the SM particles. Such light axions can be pseudo-Nambu-Goldstone-bosons (PNGB). The Peccei-Quinn symmetry U(1), $U\tilde{(1)}$ or $U(1)_{PQ}$, is explicitly broken by QCD's axial anomaly. $U(1)_{PQ}$ introduces PNGB after symmetry breaking, and this leads to a solution to the CP problem of the strong interaction [36]. Two features of those light PNGBs are

- small coupling: the spontaneous symmetry breaking suppresses their interactions,
- small mass: in the case of exact symmetry(almost unbroken symmetries), they would be massless.

ALP could be responsible for [35]

- reproduction of DM to correct relic abundance of matter
- inflation
- explaining the observed value of the muon's magnetic moment
- EW symmetry breaking in the solution of the hierarchy problem.

They can couple to two gauge bosons or couple to SM fermions. The Lagrangian of the di-photon coupled ALP is given as

$$\mathcal{L} = \frac{1}{2}\partial^{\mu}a\partial_{\mu}a - \frac{1}{2}m_a^2a^2 - \frac{1}{4}g_{a\gamma}aF^{\mu\nu}\tilde{F}_{\mu\nu} \tag{5.1}$$

The model is described by two parameters; the mass of a, m_a, and the coupling to di-photon, $g_{a\gamma}$. The coherent pN interaction, which is the proton's elastic scattering on the nucleus, can produce ALP via the Primakoff process (see Figure 5.1). The lifetime and production rate can be calculated from m_a and $g_{a\gamma}$ by doing equivalent photon approximation (EPA). This approximation is suitable for high-energetic-proton-beams having m_a more than 100MeV. Considering the interaction of two composite particles, proton and nucleus, the production procedure could be deliberative.

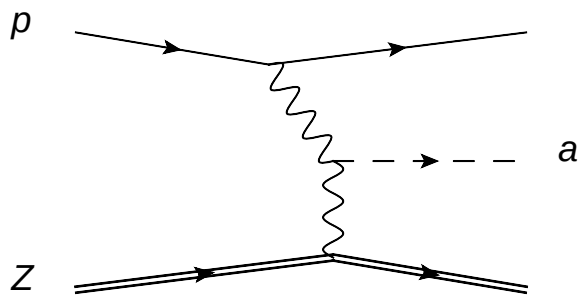

Figure 5.1: Primakoff ALP production in pN scattering

ALPACA is an ALP MC event generator written in Fortran language. It uses the Primakoff process to produce massive ALPs. ALPACA is implemented to the SHiP software by setting SHiP's material geometry; the production cross-section, σ_{ALP} is calculated. In References [1, 32], the MC event generator, ALPACA, and the model are described in more detail.

5.1 ALP Production Mechanism

When the proton's EM field interacts with the nucleus, it is called a coherent pN process. The most suitable coherent ALP production is the Primakoff ALP production, which is analogous to the Primakoff effect. Primakoff ALP production is suitable in

proton beam dump experiments due to the following reasons [1, 35]:

- The coherent cross-section scales with the particle's charged square, Z^2. Therefore, the production rate will be larger for thick targets as in the SHiP case.
- Produced ALP in this process will have small transverse momentum, enhancing the cross-section in the beam direction. Therefore, the geometric acceptance of the SHiP detector will be high for ALP events.

Strong constraints are expected for the quark coupled ALP because the flavor-changing rare decays suppress ALP production rates. On the other hand, photon coupled ALP production via the Primakoff process gives the dominant contributions [1]. In the Primakoff production, the equivalent photon spectrum of pN scattering can be calculated in the center-of-mass frame. Then, the differential cross-section can be obtained by considering the process of photon-fusion, $\gamma + \gamma \to a$. Weizsaeker-Williams EPA studies photons which are emitted from the fast charges. EPA aims to predict the angular distribution of photons accurately; then, ALP production's total cross-section in the photon fusion can be obtained [1]. EPA uses distribution functions of the photons carried by the proton and the nucleus, and this process is an analogy to Parton distribution functions in proton-proton collisions. It means that the partonic cross-section inside the box, as in Figure 5.2, is considered in the ALPACA calculations.

In ALPACA, the cross section of the ALP production is by [1]

$$\sigma_{ALP} = \int \mathrm{d}x_1 \mathrm{d}x_2 \, \mathrm{d}^2 q_{1_\perp} \mathrm{d}^2 q_{2_\perp} \, N_p(x_1, q_{1_\perp}^2) N_n(x_2, q_{2_\perp}^2) \, \sigma(\gamma\gamma \to a) \, . \tag{5.2}$$

where the di-photon to a process cross-section is

$$\sigma(\gamma\gamma \to a) = \frac{\pi g_{a\gamma\gamma}^2 m_a}{16} \delta(m_{\gamma\gamma} - m_a) \, . \tag{5.3}$$

From [1], the angular dependence on cross-section is observed as shown in Figure 5.3

The events are generated from ALPACA as in DP production. a is produced in the target with the $\pm$ 1cm beam smear, and then it decays in the vessel by decay boosting

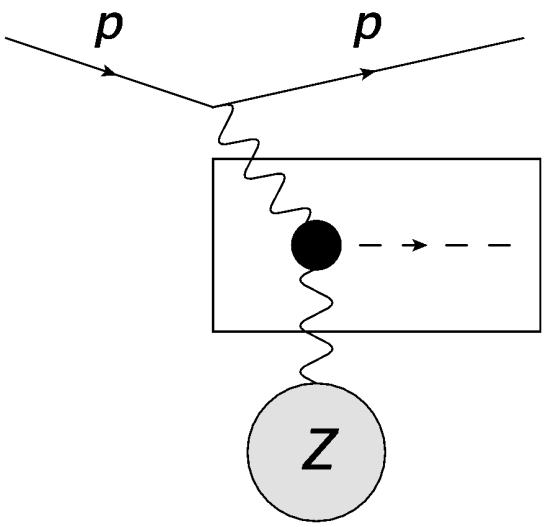

Figure 5.2: The coherent proton scattering on nucleus

factor (see Equation 4.20). Later, events are renormalized by the weight (see Equation 6.2) in the analysis procedure. The lifetime is calculated by Equation 5.5. In the final step, the decay products are interacted with the material of SHiP geometry in GEANT4.

5.2 ALP Decays

Our study aims to detect ALP from their diphoton decays in the SHiP Split Calorimeter, SplitCal [92]), which allows us to use the neutral final states (in contrast to searches of DP and HNL). The ALP decay width is given as [1, 32]:

$$\Gamma = \frac{g_{a\gamma}^2 m_a^3}{64\pi} \tag{5.4}$$

There is a cubic dependence on mass, and squared dependence on photon coupling. The lifetime is inversely proportional to the decay width:

$$l_a = \beta\gamma\tau = \frac{64\pi}{g_{a\gamma}^2 m_a^3} \tag{5.5}$$

The range of $g_{a\gamma}$ is between 10^{-2} and 10^{-8}. The process in this range requires intense proton beams and highly sensitive detectors with a clean environment to pro-

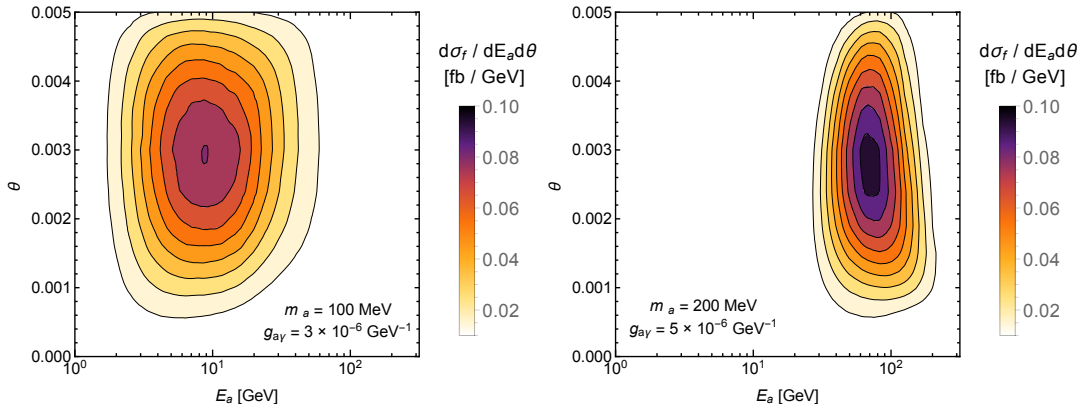

Figure 5.3: The differential cross section of a as a function of the energy and angle for different m_a and g. It is taken from [1].

duce as many ALPs as possible. Furthermore, the distance between the target and vessel entrance should be optimized. These conditions are fulfilled by NA62 [93] and SHiP [25].

5.3 Analysis

In order to obtain exclusion contours, MC events are generated according to grid points in (m_a, $g_{a\gamma}$). The mass is varied from 0.002 GeV to 1.10 GeV and coupling constant is varied logarithmically from 10^{-2} to 10^{-8}. In total, $\sim$ 800 grid points are produced, which corresponds to $\sim$ 4.5 M MC events. The selection criterias in Table 5.1 are used to find the number of selected a events in the SHiP detector. The efficiency of each step is given in Figure 5.4.

Once all the requirements are satisfied, the geometric acceptance, $\mathcal{A}_{\text{geo}}$, is defined as in Equations 4.21 and 4.22.

The kinematic selections of ALP only depend on the m_a in Figure 5.4. The vessel probability is mostly below 20-30 %. As m_a exceeds 0.3 GeV, the reconstruction efficiency is above 85%. The final kinematical selection rejects the soft particles. In Figure 5.5, 5.6, 5.7 and 5.8, 5.9, 5.10, kinematics of the final decay products are compared in three different masses before and after each selection step in Table 5.1.

Table 5.1: a selections

Decay Selection (Fig 5.4 on left)	MC vertex is inside the vessel, 6 m away from the entrance, and, before the exit, at least 5 cm away from its inner walls in X and Y
Passing Tracker Stations(Fig 5.4 on middle)	two γ final products are extrapolated to the SplitCAL.
Final Selection (Fig 5.4 on right)	DOCA < 1 cm, P > 1GeV

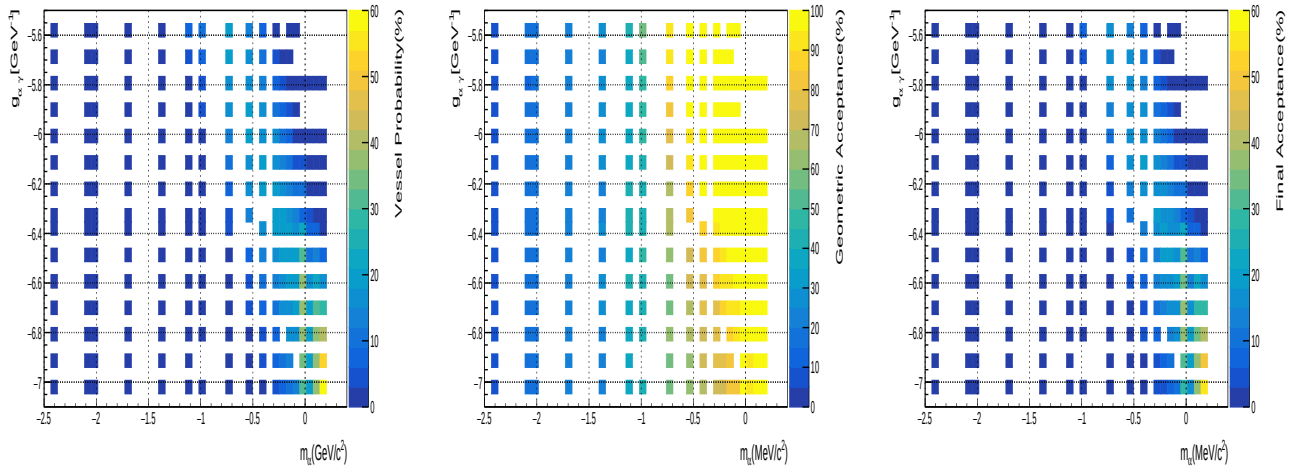

Figure 5.4: Vessel Probability, Geometric Acceptance and Final Acceptance of a events as a function of m$_a$ and $g_{a\gamma}$

The angular distribution dependence on the a decay products is observed.

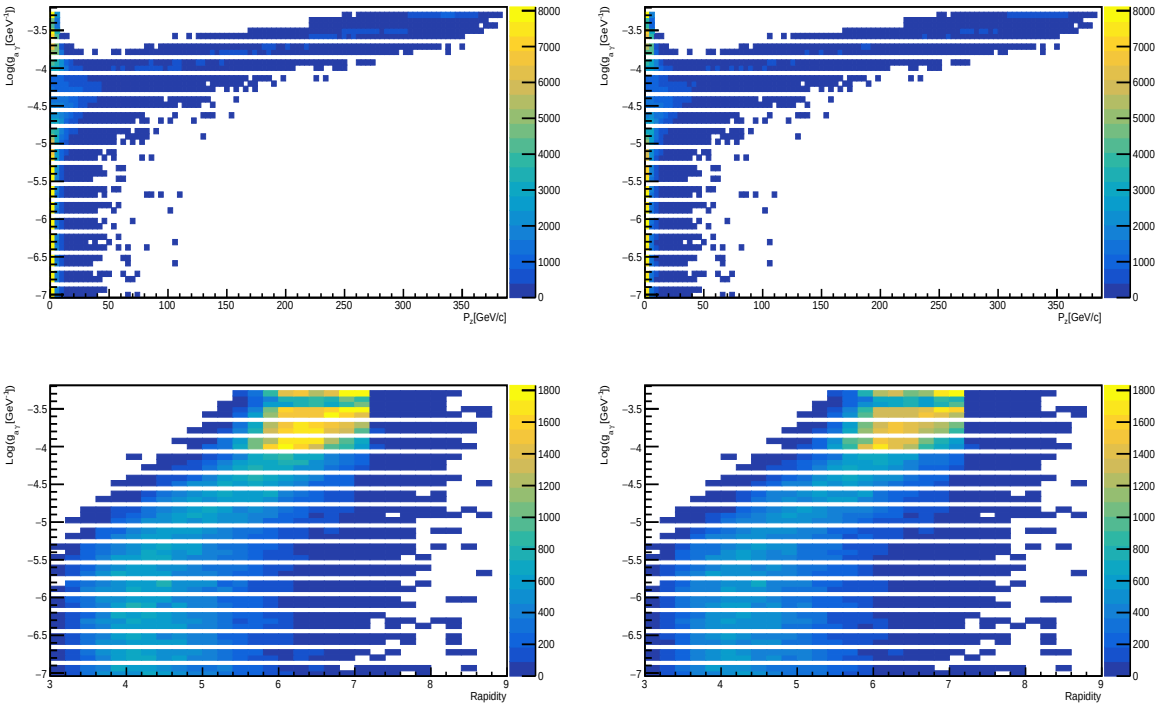

Figure 5.5: ε versus P_z and ε versus rapidity distributions of the decay products at the m_a = 0.08 GeV. On left: the purified events. On right: the vessel selected events

5.3.1 Estimation of Exclusion Contours

In order to obtain the a exclusion contour, the geometric acceptance, $\mathcal{A}_{\text{geo}}$ (see Equation 4.21), and the production cross-section, σ_{ALP} (see Equation 5.2), are used to get the number of detected events, $\mathcal{N}_a$ (see Equation 6.1), at each grid point in (m_a, $g_{a\gamma}$). A lower coupling limit and an upper coupling limit are then calculated for each mass point by assuming a 90% confidence limit. As an example, the limits obtained for three different masses are shown in Figure 5.11. The ROOT class TEVAL is used for the limit estimation.

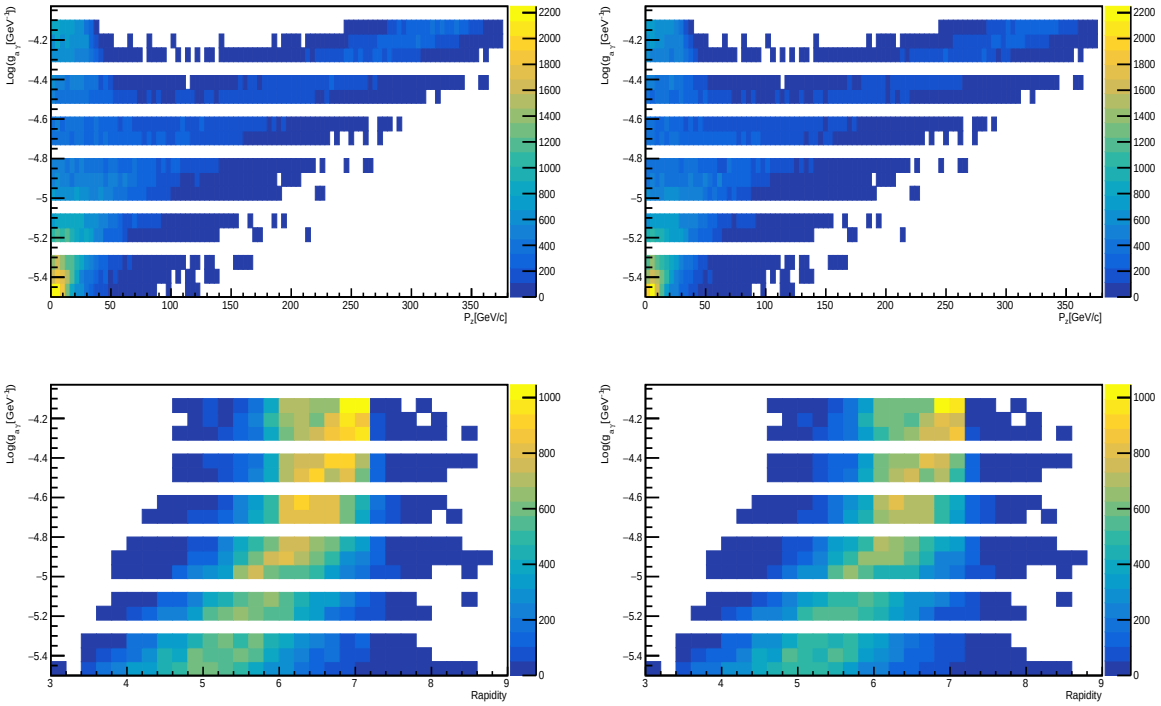

Figure 5.6: ε versus P_z and ε versus rapidity distributions of the decay products at the m_a = 0.2 GeV. On left: the purified events. On right: the vessel selected events

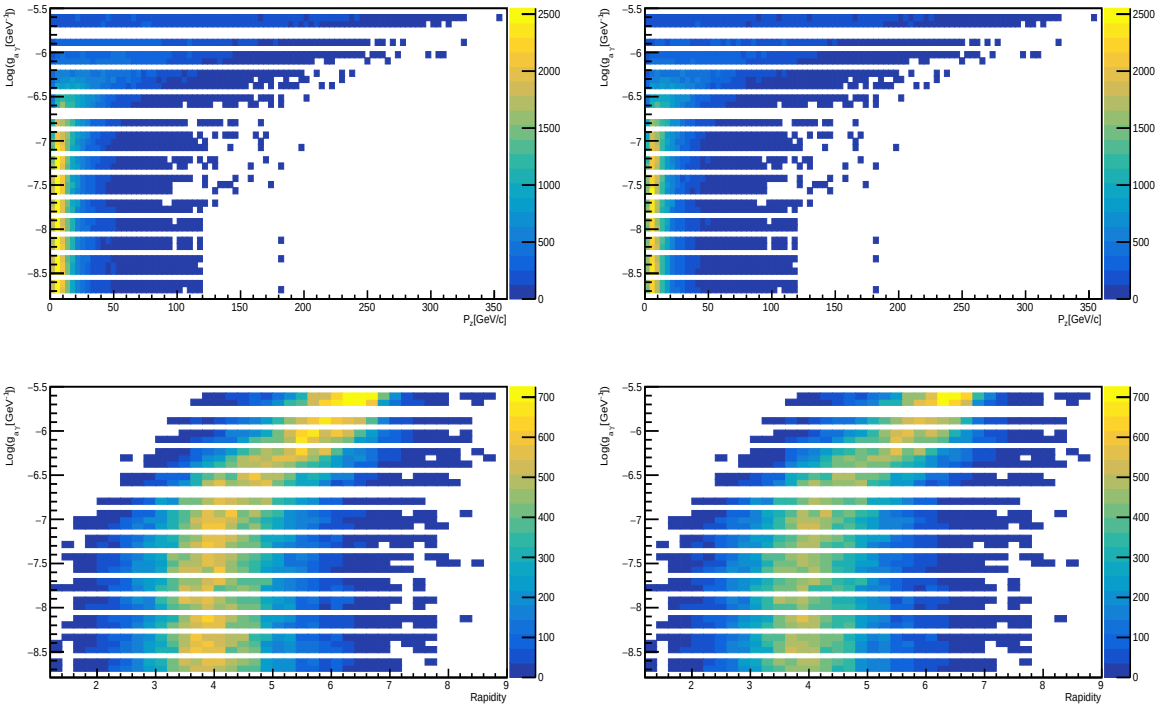

Figure 5.7: ε versus P_z and ε versus rapidity distributions of the decay products at the m_a = 0.8 GeV. On left: the purified events. On right: the vessel selected events

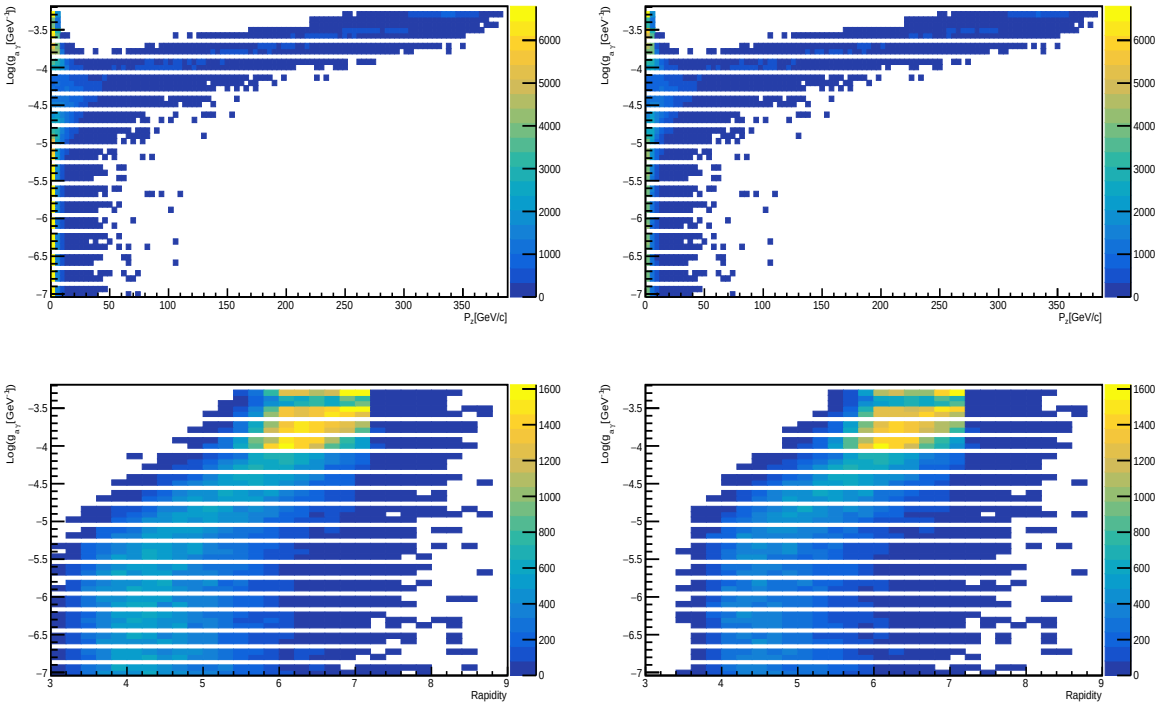

Figure 5.8: ε versus P_z and ε versus rapidity distributions of the decay products at the m_a = 0.08 GeV. On left: the vessel selected events. On right: the final selected events

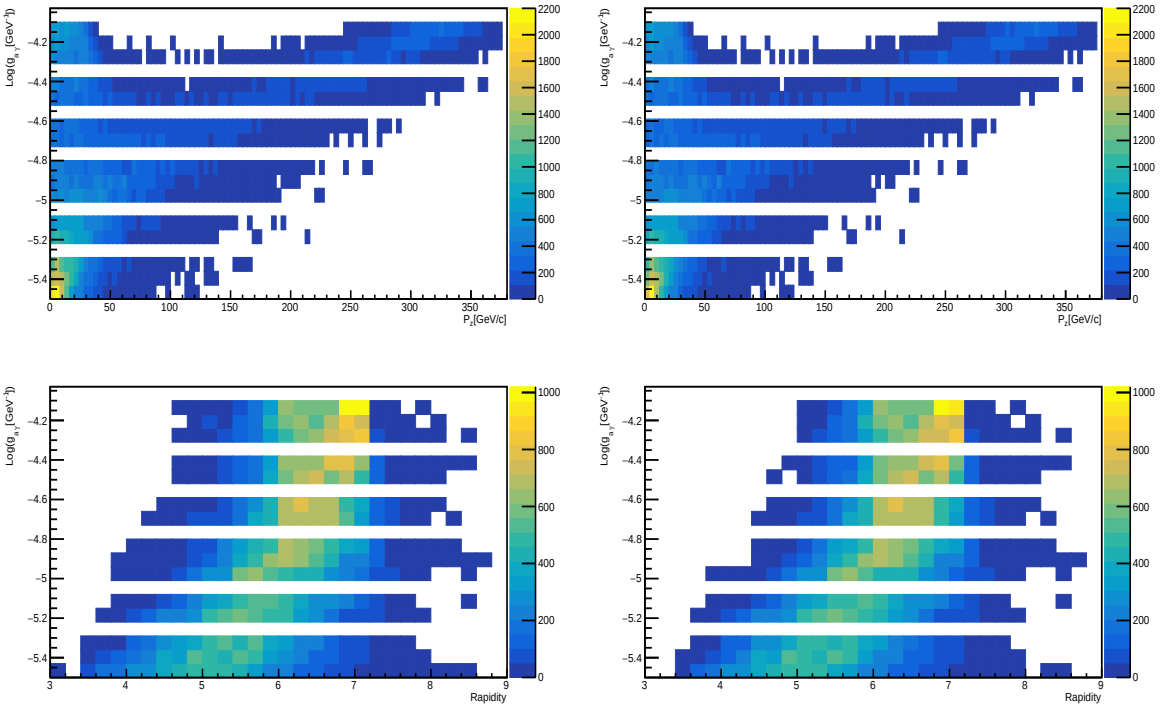

Figure 5.9: ε versus P_z and ε versus rapidity distributions of the decay products at the m_a = 0.2 GeV. On left: the vessel selected events. On right: the final selected events

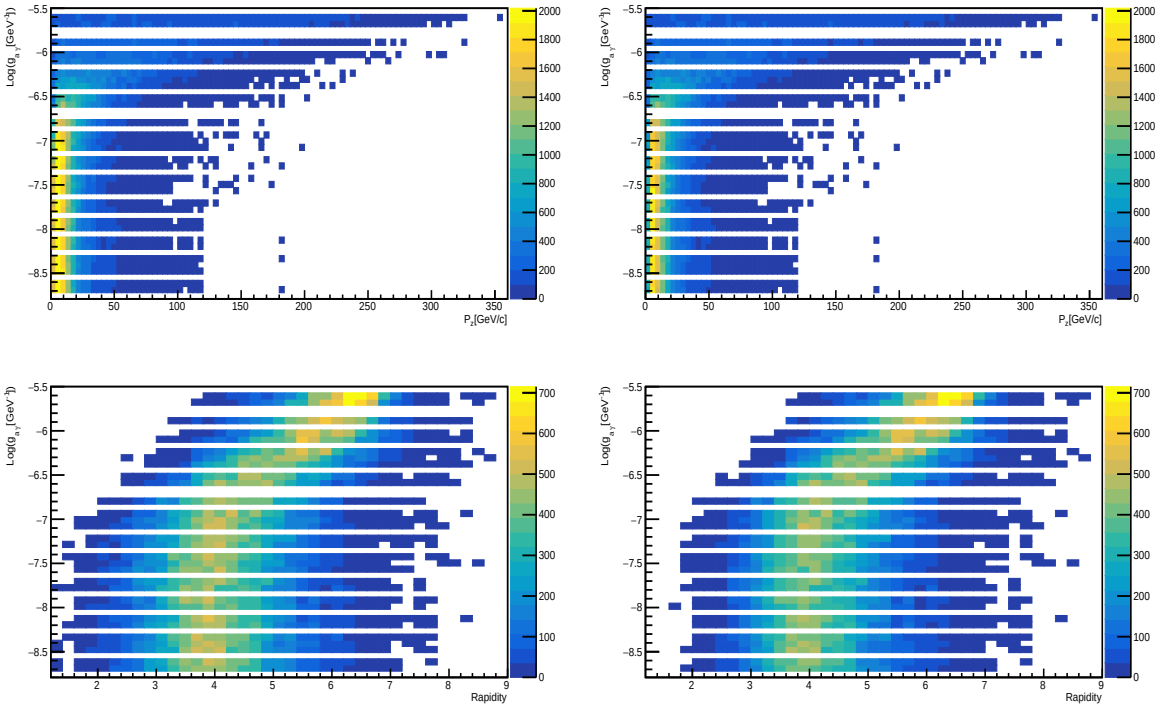

Figure 5.10: ε versus P_z and ε versus rapidity distributions of the decay products at the m_a = 0.8 GeV. On left: the vessel selected events. On right: the final selected events

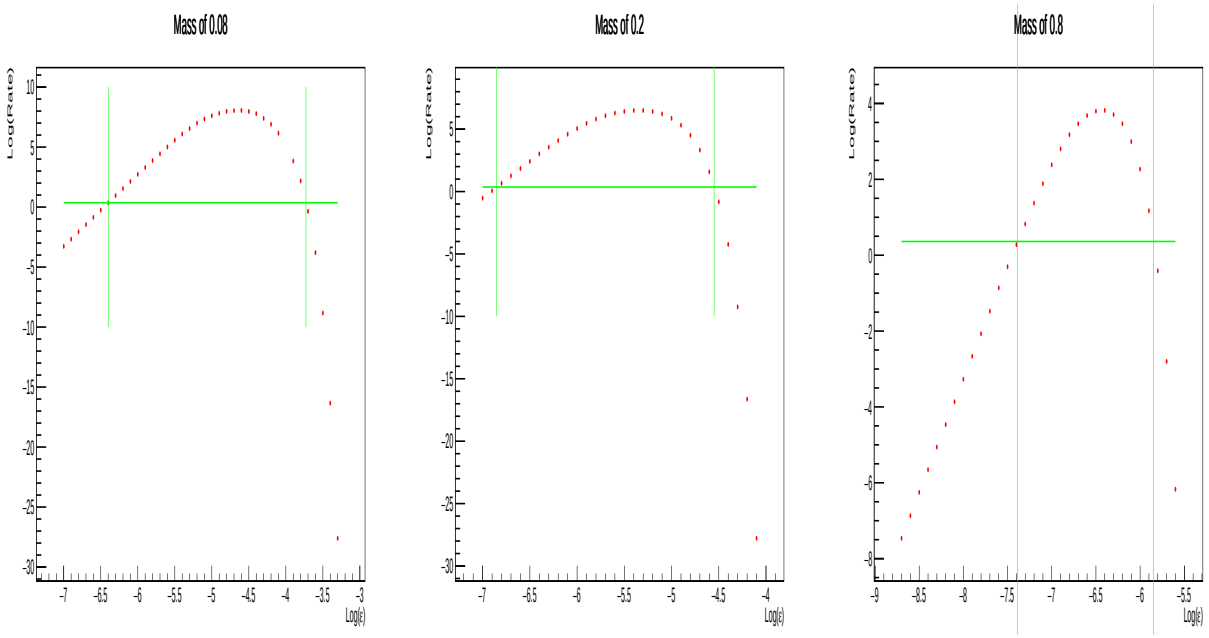

Figure 5.11: The lower and upper limits of $g_{a\gamma}$ (vertical green lines) for three different m_a values.

CHAPTER 6

RESULTS & CONCLUSION

This thesis work estimates the sensitivity of the SHiP experiment for DP and ALP searches. The sensitivity limit is evaluated via null-hypothesis testing under the assumption of 2×10^{20} p.o.t. with 0.1 background.

6.1 Sensitivity Contours

First of all, if there is no discovery, it does not mean failure. It would not be correct to say that the particle does not exist or its cross-section vanishes; this negative result could be considered as a production limit. The particle may still exist, but the production rate can be too small to be observed in the experiment. The number of observed events is described by a Poisson distribution [94]:

$$r_P(n=0|N_{lim}) = \frac{(N_{lim})^0 e^{-N_{lim}}}{n!} = e^{-N_{lim}} = 0.1 \; ; \; N_{lim} = -ln(0.1) = 2.3$$

where n is the number of observed events, N_{lim} is the expected number of background events (background events that pass through all selection criterion). So, $N_{lim} = 2.3$ events becomes the expected number of background events for 90% confidence interval [95]. To sum up, there are two possible outcomes in this study [27, 67]:

1. If no event is observed in the phase-space that SHiP is sensitive, the region can be excluded with a 90% confidence interval.

2. On the other hand, if two events are observed, the contour will be represented as a discovery region with 3σ [67, 96].

In order to explore the region where SHiP is sensitive to the hidden particles, the expected number of events is evaluated by [16, 27, 97]:

$$\mathcal{N}_X = \sigma_{\rm prod} \times \mathcal{L}_{\rm SHiP} \times {\rm BR}(X \to \text{visible channels}) \times \mathcal{A}_{\rm geo}, . \tag{6.1}$$

$$\mathcal{L}_{\rm SHiP} = \frac{\rm N_{p.o.t.}}{\sigma^{\rm inelastic}_{SHiP}} \text{ where } \rm N_{p.o.t.} = 2 \times 10^{20} \text{ and } \sigma^{\rm inelastic}_{SHiP} = \frac{\rm m_{proton}}{\Lambda^{\rm Mo}_{\rm I}} \approx 10.7 \text{ mb} .$$

$\mathcal{N}_X$ is the expected number of event for five years run of SHiP and $\sigma_{\rm mode}$ is the cross-section for the responsible production mechanisms of the hidden particles (see Equations 4.5, 4.10, 4.11, 5.2). $\mathcal{L}_{\rm SHiP}$ is the fixed-target luminosity [53]; $\sigma^{inelastic}_{SHiP}$ is the proton-nucleus cross section of Molybdenum target where Λ^{Mo}_{I} is taken from [79] (see Table 3.1). $\mathcal{A}_{geo}$ is the geometric acceptance which is vessel probability times reconstruction efficiency (see Equation 4.21). The weight factor of $\rm w_{vtx}(\ell)$ is given by [27, 39, 42, 73]:

$$\rm w_{vtx}(\ell) = e^{-\frac{\ell + L_0}{\beta x \gamma \times c\tau}} \times \frac{1}{\beta \times \gamma \times c\tau} \tag{6.2}$$

where $\gamma = E_X/\sqrt{E^2_X - p^2_X}, \beta = p_X/E_X$, $\rm L_0$ is the distance between starting z point of decay vessel and the target, and ℓ is the randomly assigned length in the decay vessel regions. Therefore, each generated MC event has a hidden particle, which is produced in the target, and its direct daughters, which are boosted to be produced inside the vessel (see Equation 4.20); this method is applied in order to gain statistics about the observable events. Later the events are normalized by the corresponding weights, $\rm w_{vtx}(\ell)$.

6.2 Exclusion plots

Once the limits are estimated in Chapters 4 and 5, they are plotted as exclusion plots in logarithmic scales of mass and coupling. As stated in [97] and explained above, the upper bound is limited by the decay length while the lower bound limit refers to the insensitive region when the hidden decay is too rare; on the other hand, the endpoint shows the mass limit of the detector.

The exclusion contours of DP searches in the SHiP experiment are shown in Figures 6.1 and 6.2. Figure 6.1 represents the contours of each production mode, and their combined contours are represented in Figure 6.2. The DP exclusion plots range from 0.002 GeV to 3.3 GeV in m_{γ^D} and 10^{-5} to 10^{-17} in ε^2. The secondary meson's EM decay production (red) is dominant until the mass of η, then, quasi-elastic scattering of incident pN (proton-bremsstrahlung (magenta and olive)) becomes dominant, and pbrem makes some resonances at about 0.8 GeV (mass of ω). The pbrem VMD FF (olive) dominates the pbrem dipole FF (magenta) at about 0.8 GeV and between 1.25 and 1.40 GeV. Then, above 1.5 GeV, the direct perturbative QCD production (blue) dominates the other modes. To sum up, DPexclusion regions in Figures 6.1 and 6.2 show the SHiP experiment sensitivity to DP from primary pN interactions. The contour promises a unique discovery potential when it is compared with other experiments [18, 19, 22, 25, 28, 31, 33, 37–39, 42, 71, 76–78, 86, 91, 98–108].

In addition to dark photon, the ALP discovery potential is also studied for the SHiP case. The exclusion contour for the ALP search is obtained and shown in Figure 6.3. The ALP sensitivity is studied at MC true level. This study will be updated once the Split Calorimeter reconstruction is ready. Nevertheless, the SHiP sensitivity offers a clear phase-space to investigate discovery potential as seen in [1, 32, 35]. It ranges from 0.01 GeV to 1.1 GeV in m_a and 10^{-2} to around 10^{-8} in $g_{a\gamma}$. In addition to SHiP, there are proposed experiments to search for ALP through visible and invible decay modes. For example, SHiP and LDMX present complementary searches in larger masses and smaller couplings of ALP.

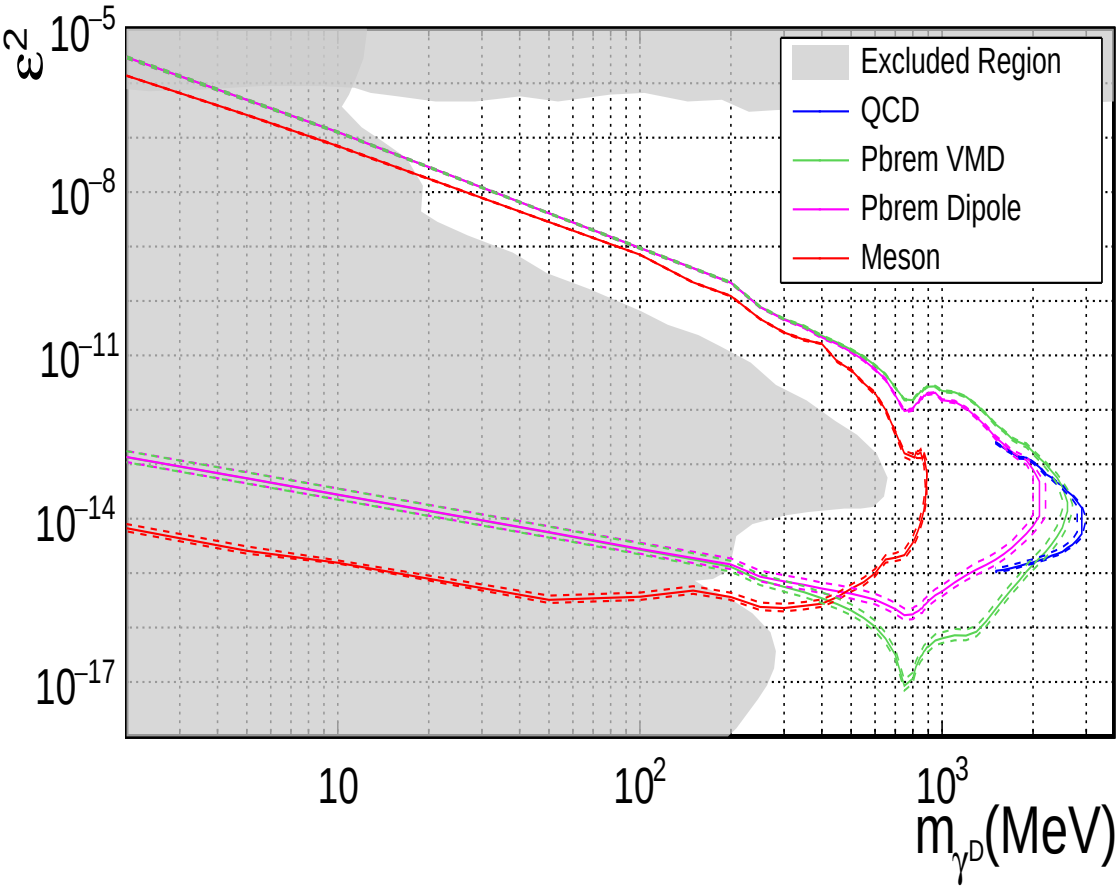

Figure 6.1: The exclusion contour for dark photon search through different production mechanisms at SHiP.

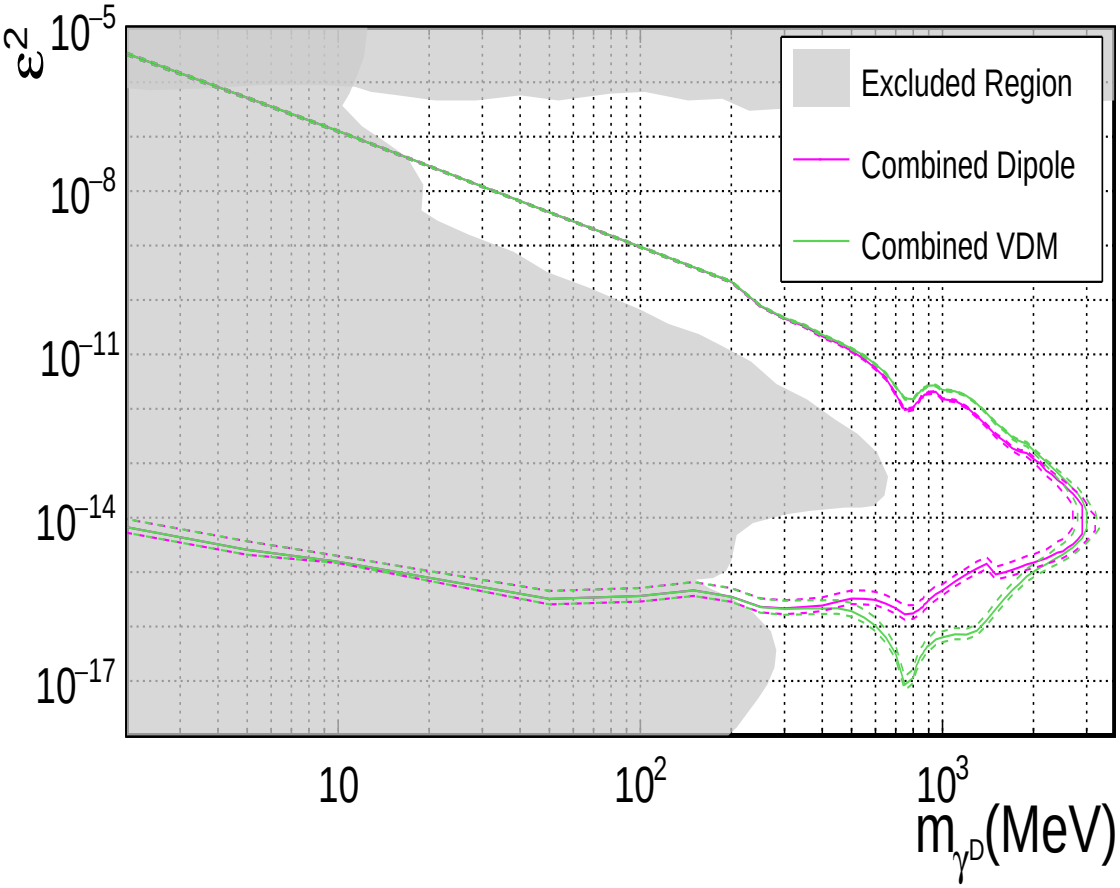

Figure 6.2: The combined exclusion contour for the dark photon search at SHiP.

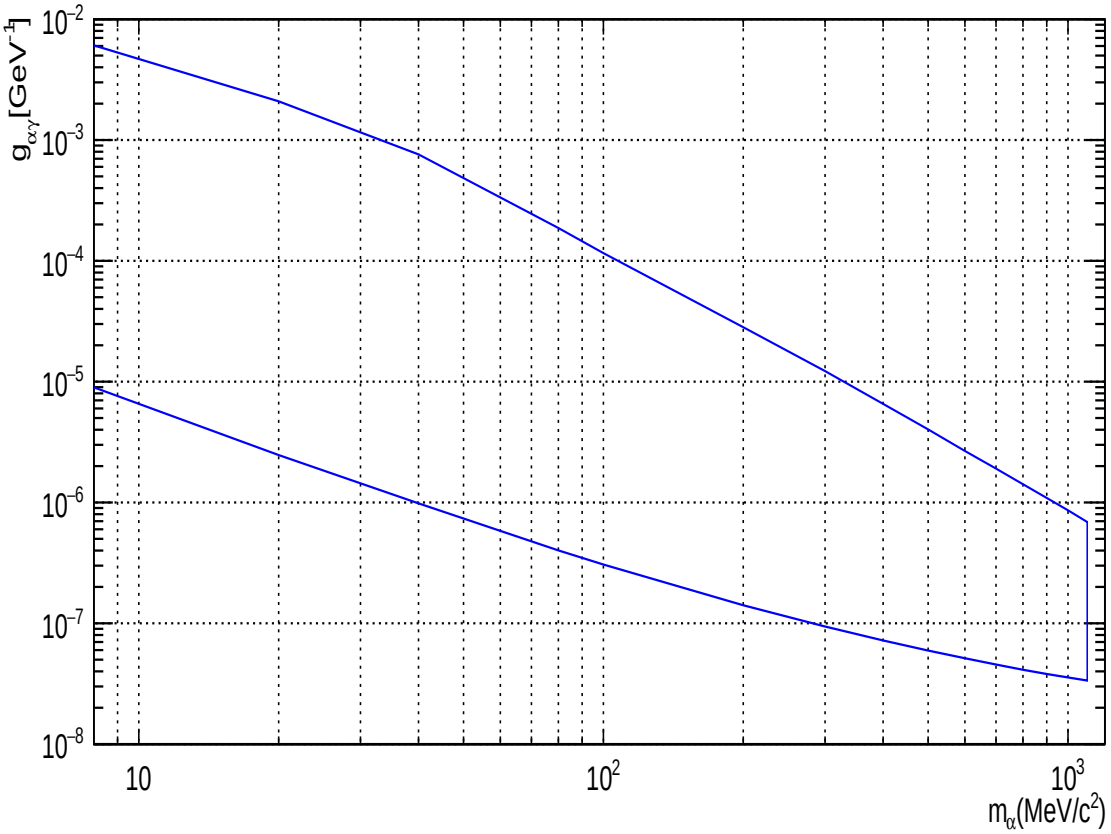

Figure 6.3: The exclusion contour for the ALP search at SHiP.

REFERENCES

[1] B. Döbrich *et al.*, "Alptraum: Alp production in proton beam dump experiments," *Journal of High Energy Physics*, vol. 2016, Feb 2016.

[2] R. P. Feynman and M. Gell-Mann, "Theory of the fermi interaction," *Phys. Rev.*, vol. 109, pp. 193–198, Jan 1958.

[3] M. Gell-Mann, "The Eightfold Way: A Theory of strong interaction symmetry," 3 1961.

[4] S. L. Glashow, "Partial-symmetries of weak interactions," *Nuclear Physics*, vol. 22, no. 4, pp. 579 – 588, 1961.

[5] Y. Nambu and G. Jona-Lasinio, "Dynamical Model of Elementary Particles Based on an Analogy with Superconductivity. 1.," *Phys. Rev.*, vol. 122, pp. 345–358, 1961.

[6] M. Banner *et al.*, "Observation of single isolated electrons of high transverse momentum in events with missing transverse energy at the cern pp collider," *Physics Letters B*, vol. 122, no. 5, pp. 476 – 485, 1983.

[7] G. Arnison *et al.*, "Experimental observation of isolated large transverse energy electrons with associated missing energy at s=540 gev," *Physics Letters B*, vol. 122, no. 1, pp. 103 – 116, 1983.

[8] G. Aad *et al.*, "Combined search for the standard model higgs boson using up to 4.9 fb-1 of pp collision data at sqrt(s) = 7 tev with the atlas detector at the lhc," *Physics Letters B*, vol. 710, pp. 49–66, Mar 2012.

[9] G. Aad *et al.*, "Observation of a new particle in the search for the standard model higgs boson with the atlas detector at the lhc," *Physics Letters B*, vol. 716, pp. 1–29, Sep 2012.

[10] S. Chatrchyan *et al.*, "Observation of a new boson at a mass of 125 gev with the cms experiment at the lhc," *Physics Letters B*, vol. 716, pp. 30–61, Sep 2012.

[11] S. Chatrchyan *et al.*, "Combined results of searches for the standard model higgs boson in pp collisions at sqrt(s) = 7 tev," *Physics Letters B*, vol. 710, pp. 26–48, Mar 2012.

[12] J. Goldstone, A. Salam, and S. Weinberg, "Broken symmetries," *Phys. Rev.*, vol. 127, pp. 965–970, Aug 1962.

[13] A. Salam and J. Ward, "Electromagnetic and weak interactions," *Physics Letters*, vol. 13, no. 2, pp. 168 – 171, 1964.

[14] P. W. Higgs, "Broken symmetries, massless particles and gauge fields," *Phys. Lett.*, vol. 12, pp. 132–133, 1964.

[15] P. W. Higgs, "Broken symmetries and the masses of gauge bosons," *Phys. Rev. Lett.*, vol. 13, pp. 508–509, Oct 1964.

[16] S. Collaboration, "A facility to Search for Hidden Particles (SHiP) at the CERN SPS," *CERN CDS*, 2015.

[17] S. Alekhin *et al.*, "A facility to Search for Hidden Particles at the CERN SPS: the SHiP physics case," *CERN CDS*, 2015.

[18] C. Ahdida *et al.*, "SHiP Experiment - Progress Report," Tech. Rep. CERN-SPSC-2019-010. SPSC-SR-248, CERN, Geneva, Jan 2019.

[19] J. Beacham *et al.*, "Physics beyond colliders at cern: beyond the standard model working group report," *Journal of Physics G: Nuclear and Particle Physics*, vol. 47, p. 010501, Dec 2019.

[20] B. Batell, M. Pospelov, and A. Ritz, "Exploring portals to a hidden sector through fixed targets," *Physical Review D*, vol. 80, Nov 2009.

[21] D. Gorbunov, A. Makarov, and I. Timiryasov, "Decaying light particles in the ship experiment: Signal rate estimates for hidden photons," *Phys. Rev. D*, vol. 91, p. 035027, Feb 2015.

[22] E. Nardi, C. D. Carvajal, A. Ghoshal, D. Meloni, and M. Raggi, "Resonant production of dark photons in positron beam dump experiments," *Physical Review D*, vol. 97, May 2018.

[23] W. Bonivento, A. Boyarsky, H. Dijkstra, U. Egede, M. Ferro-Luzzi, B. Goddard, A. Golutvin, D. Gorbunov, R. Jacobsson, J. Panman, M. Patel, O. Ruchayskiy, T. Ruf, N. Serra, M. Shaposhnikov, and D. Treille, "Proposal to search for heavy neutral leptons at the sps," 2013.

[24] C. C. Ahdida *et al.*, "A Beam Dump Facility (BDF) at CERN – The Concept and a First Radiological Assessment ," Tech. Rep. CERN-PBC-CONF-2019-001, CERN, Geneva, Jan 2019.

[25] C. Ahdida *et al.*, "SHiP Experiment - Comprehensive Design Study report," Tech. Rep. CERN-SPSC-2019-049. SPSC-SR-263, CERN, Geneva, Dec 2019.

[26] C. Ahdida *et al.*, "SPS Beam Dump Facility - Comprehensive Design Study," Dec 2019.

[27] S. Colloboration, "Sensitivity of the ship experiment to dark photons decaying to a pair of charged particles," *Submitted to EPJC*, 2020.

[28] R. Essig *et al.*, "Dark sectors and new light weakly-coupled particles," 2013.

[29] J. Jaeckel and A. Ringwald, "The low-energy frontier of particle physics," *Annual Review of Nuclear and Particle Science*, vol. 60, pp. 405–437, Nov 2010.

[30] B. Batell, M. Pospelov, and A. Ritz, "Exploring Portals to a Hidden Sector Through Fixed Targets," *Phys. Rev.*, vol. D80, p. 095024, 2009.

[31] A. Fradette, M. Pospelov, J. Pradler, and A. Ritz, "Cosmological constraints on very dark photons," *Physical Review D*, vol. 90, Aug 2014.

[32] L. Harland-Lang, J. Jaeckel, and M. Spannowsky, "A fresh look at alp searches in fixed target experiments," *Physics Letters B*, vol. 793, pp. 281–289, Jun 2019.

[33] J. L. Feng, I. Galon, F. Kling, and S. Trojanowski, "Axionlike particles at faser: The lhc as a photon beam dump," *Physical Review D*, vol. 98, Sep 2018.

[34] Y. Nomura and J. Thaler, "Dark matter through the axion portal," *Physical Review D*, vol. 79, Apr 2009.

[35] B. Döbrich, J. Jaeckel, and T. Spadaro, "Light in the beam dump. axion-like particle production from decay photons in proton beam-dumps," *Journal of High Energy Physics*, vol. 2019, no. 5, p. 213, 2019.

[36] K. Kaneta, H.-S. Lee, and S. Yun, "Portal connecting dark photons and axions," *Physical Review Letters*, vol. 118, Mar 2017.

[37] P. Ilten, Y. Soreq, J. Thaler, M. Williams, and W. Xue, "Proposed inclusive dark photon search at lhcb," *Phys. Rev. Lett.*, vol. 116, p. 251803, Jun 2016.

[38] S. Abrahamyan *et al.*, "Search for a new gauge boson in electron-nucleus fixed-target scattering by the apex experiment," *Physical Review Letters*, vol. 107, Nov 2011.

[39] J. D. Bjorken, R. Essig, P. Schuster, and N. Toro, "New Fixed-Target Experiments to Search for Dark Gauge Forces," *Phys. Rev.*, vol. D80, p. 075018, 2009.

[40] S. Bilmiş, I. Turan, T. Aliev, M. Deniz, L. Singh, and H. Wong, "Constraints on dark photon from neutrino-electron scattering experiments," *Physical Review D*, vol. 92, Aug 2015.

[41] S. N. Gninenko, "Stringent limits on the $\pi^0 \to \gamma x$, $x \to e^+e^-$ decay from neutrino experiments and constraints on new light gauge bosons," *Phys. Rev. D*, vol. 85, p. 055027, Mar 2012.

[42] S. Andreas, C. Niebuhr, and A. Ringwald, "New limits on hidden photons from past electron beam dumps," *Physical Review D*, vol. 86, Nov 2012.

[43] J. Blümlein *et al.*, "Limits on neutral light scalar and pseudoscalar particles in a proton beam dump experiment," *Zeitschrift für Physik C Particles and Fields*, vol. 51, no. 3, pp. 341–350, 1991.

[44] R. Essig, R. Harnik, J. Kaplan, and N. Toro, "Discovering new light states at neutrino experiments," *Physical Review D*, vol. 82, Dec 2010.

[45] S. Chatrchyan, V. Khachatryan, A. Sirunyan, A. Tumasyan, W. Adam, E. Aguilo, T. Bergauer, M. Dragicevic, J. Erö, C. Fabjan, and et al., "Observation of a new boson at a mass of 125 gev with the cms experiment at the lhc," *Physics Letters B*, vol. 716, p. 30–61, Sep 2012.

[46] G. Degrassi, S. Di Vita, J. Elias-Miró, J. R. Espinosa, G. F. Giudice, G. Isidori, and A. Strumia, "Higgs mass and vacuum stability in the standard model at nnlo," *Journal of High Energy Physics*, vol. 2012, Aug 2012.

[47] F. Bezrukov, M. Y. Kalmykov, B. A. Kniehl, and M. Shaposhnikov, "Higgs boson mass and new physics," *Journal of High Energy Physics*, vol. 2012, Oct 2012.

[48] D. Buttazzo, G. Degrassi, P. P. Giardino, G. F. Giudice, F. Sala, A. Salvio, and A. Strumia, "Investigating the near-criticality of the higgs boson," *Journal of High Energy Physics*, vol. 2013, Dec 2013.

[49] F. Bezrukov, J. Rubio, and M. Shaposhnikov, "Living beyond the edge: Higgs inflation and vacuum metastability," *Physical Review D*, vol. 92, Oct 2015.

[50] F. Bezrukov and M. Shaposhnikov, "Why should we care about the top quark yukawa coupling?," *Journal of Experimental and Theoretical Physics*, vol. 120, p. 335–343, Mar 2015.

[51] A. Akmete *et al.*, "The active muon shield in the ship experiment," *Journal of Instrumentation*, vol. 12, pp. P05011–P05011, May 2017.

[52] O. Lantwin, "Optimisation of the SHiP experimental design," 2019. Presented 09 May 2019.

[53] W. Herr and B. Muratori, "Concept of luminosity," in *CERN Accelerator School and DESY Zeuthen: Accelerator Physics*, pp. 361–377, 9 2003.

[54] C. Ahdida *et al.*, "Measurement of the muon flux for the SHiP experiment," Tech. Rep. CERN-EP-2020-006, CERN, Geneva, 1 2020.

[55] C. Ahdida *et al.*, "Measurement of the muon flux from 400 gev/c protons interacting in a thick molybdenum/tungsten target," *The European Physical Journal C*, vol. 80, no. 3, p. 284, 2020.

[56] B. Hosseini and W. M. Bonivento, "Particle Identification tools and performance in the SHiP Experiment," *CERN CDS*, Jul 2017.

[57] I. Bereziuk, O. Bezshyyko, and M. Ferro-Luzzi, "Initial design studies of the SHiP straw detector," Mar 2015.

[58] E. Van Herwijnen, H. Dijkstra, M. Ferro-Luzzi, and T. Ruf, "Simulation and pattern recognition for the SHiP Spectrometer Tracker," *CERN CDS*, Mar 2015.

[59] M. Al-Turany *et al.*, "The fairroot framework," *Journal of Physics: Conference Series*, vol. 396, no. 2, p. 022001, 2012.

[60] T. Sjöstrand *et al.*, "An Introduction to PYTHIA 8.2," *Comput. Phys. Commun.*, vol. 191, pp. 159–177, 2015.

[61] T. Sjöstrand, S. Mrenna, and P. Z. Skands, "Pythia 6.4 physics and manual," *Journal of High Energy Physics*, vol. 2006, no. 05, p. 026, 2006.

[62] S. Agostinelli *et al.*, "GEANT4: A Simulation toolkit," *Nucl. Instrum. Meth.*, vol. A506, p. 250, 2003.

[63] C. Andreopoulos *et al.*, "The GENIE Neutrino Monte Carlo Generator," *Nucl. Instrum. Meth.*, vol. A614, pp. 87–104, 2010.

[64] S. Collaboration, "Heavy Flavour Cascade Production in a Beam Dump," *CERN CDS*, Dec 2015.

[65] T. Ruf and E. Van Herwijnen, "Description of the SHiP FixedTargetGenerator," *CERN CDS*, Aug 2017.

[66] E. Graverini, N. Serra, and B. Storaci, "Search for new physics in ship and at future colliders," 2015.

[67] E. Graverini, "SHiP sensitivity to Dark Photons," *CERN CDS*, Sep 2016.

[68] L. Okun, "LIMITS OF ELECTRODYNAMICS: PARAPHOTONS?," *Sov. Phys. JETP*, vol. 56, p. 502, 1982.

[69] B. Holdom, "Two U(1)'s and Epsilon Charge Shifts," *Phys. Lett.*, vol. 166B, pp. 196–198, 1986.

[70] B. Holdom, "Searching for epsilon charges and a new u(1)," *Physics Letters B*, vol. 178, no. 1, pp. 65 – 70, 1986.

[71] M. Reece and L.-T. Wang, "Searching for the light dark gauge boson in gev-scale experiments," *Journal of High Energy Physics*, vol. 2009, pp. 051–051, Jul 2009.

[72] L. Carloni, J. Rathsman, and T. Sjöstrand, "Discerning Secluded Sector gauge structures," *JHEP*, vol. 04, p. 091, 2011.

[73] M. Raggi and V. Kozhuharov, "Results and perspectives in dark photon physics," *Riv. Nuovo Cim.*, vol. 38, no. 10, pp. 449–505, 2015.

[74] J. Blümlein and J. Brunner, "New Exclusion Limits on Dark Gauge Forces from Proton Bremsstrahlung in Beam-Dump Data," *Phys. Lett.*, vol. B731, pp. 320–326, 2014.

[75] J. Blümlein and J. Brunner, "New exclusion limits for dark gauge forces from beam-dump data," *Physics Letters B*, vol. 701, pp. 155–159, Jul 2011.

[76] H. Merkel, P. Achenbach, C. Ayerbe Gayoso, J. C. Bernauer, R. Böhm, D. Bosnar, L. Debenjak, A. Denig, M. O. Distler, A. Esser, and et al., "Search for light gauge bosons of the dark sector at the mainz microtron," *Physical Review Letters*, vol. 106, Jun 2011.

[77] S. CHOI, "Searches for the dark photon at fixed target experiments," *The origin of New Physics: Sae Mulli*, vol. 66, pp. 1036–1044, 08 2016.

[78] C. Bravo, "The heavy photon search experiment," 2019.

[79] C. Patrignani *et al.*, "Review of Particle Physics," *Chin. Phys.*, vol. C40, no. 10, p. 100001, 2016.

[80] D. Gorbunov, A. Makarov, and I. Timiryasov, "Decaying light particles in the SHiP experiment: Signal rate estimates for hidden photons," *Phys. Rev.*, vol. D91, no. 3, p. 035027, 2015.

[81] P. deNiverville, C.-Y. Chen, M. Pospelov, and A. Ritz, "Light dark matter in neutrino beams: production modelling and scattering signatures at MiniBooNE, T2K and SHiP," *Phys. Rev.*, vol. D95, no. 3, p. 035006, 2017.

[82] A. Faessler, M. I. Krivoruchenko, and B. V. Martemyanov, "Once more on electromagnetic form factors of nucleons in extended vector meson dominance model," *Phys. Rev.*, vol. C82, p. 038201, 2010.

[83] L. N. Hand, D. G. Miller, and R. Wilson, "Electric and magnetic form factors of the nucleon," *Rev. Mod. Phys.*, vol. 35, p. 335, Apr 1963.

[84] K. Nakamura *et al.*, "Review of Particle Physics," *Journal of Physics G: Nuclear and Particle Physics*, vol. 37, no. 7A, p. 075021, 2010.

[85] S. Prasad and J.-C. Peng, "Dark Photon Search with Drell-Yan-Like Process," in *APS Division of Nuclear Physics Meeting Abstracts*, vol. 2015 of *APS Meeting Abstracts*, p. ND.002, Oct. 2015.

[86] S. Gardner, R. Holt, and A. Tadepalli, "New prospects in fixed target searches for dark forces with the seaquest experiment at fermilab," *Physical Review D*, vol. 93, Jun 2016.

[87] L. Carloni, J. Rathsman, and T. Sjostrand, "Discerning Secluded Sector gauge structures," *JHEP*, vol. 04, p. 091, 2011.

[88] C. Ciobanu, T. Junk, G. Veramendi, J. Lee, G. De Lentdecker, K. S. McFarland, and K. Maeshima, "Z' generation with PYTHIA," 2005.

[89] A. Akmete, A. M. Magnan, and A. M. Güler, "Update on dark photon study," (https://indico.cern.ch/event/705102/contributions/2920303/), SHiP Experiment, CERN, March 2018.

[90] F. Halzen and A. D. Martin, *QUARKS AND LEPTONS: AN INTRODUCTORY COURSE IN MODERN PARTICLE PHYSICS*. 1 1984.

[91] M. X. Liu, "Prospects of direct search for dark photon and dark higgs in seaquest/e1067 experiment at the fermilab main injector," *Modern Physics Letters A*, vol. 32, no. 10, p. 1730008, 2017.

[92] W. M. Bonivento, "Studies for the electro-magnetic calorimeter SplitCal for the SHiP experiment at CERN with shower direction reconstruction capability," *Journal of Instrumentation*, vol. 13, pp. C02041–C02041, feb 2018.

[93] E. Goudzovski, "Searches for physics beyond the standard model with kaons at na48 and na62 at cern," 2008.

[94] C. A. Pruneau, *Data Analysis Techniques for Physical Scientists*. Cambridge University Press, 2017.

[95] R. M. Barnett and et al., "Review of particle physics," *Phys. Rev. D*, vol. 54, pp. 1–708, Jul 1996.

[96] S. Gninenko, "Constraints on sub-gev hidden sector gauge bosons from a search for heavy neutrino decays," *Physics Letters B*, vol. 713, pp. 244–248, Jul 2012.

[97] K. Bondarenko *et al.*, "Sensitivity of the intensity frontier experiments for neutrino and scalar portals: analytic estimates," *Journal of High Energy Physics*, vol. 2019, Aug 2019.

[98] J. Jaeckel, M. Lamont, and C. Vallée, "The quest for new physics with the physics beyond colliders programme," *Nature Physics*, vol. 16, no. 4, pp. 393–401, 2020.

[99] H. Merkel *et al.*, "Search for light gauge bosons of the dark sector at the mainz microtron," *Physical Review Letters*, vol. 106, Jun 2011.

[100] S. Andreas *et al.*, "Proposal for an experiment to search for light dark matter at the sps," 2013.

[101] J. Balewski *et al.*, "The darklight experiment: A precision search for new physics at low energies," 2014.

[102] J. Lees, V. Poireau, V. Tisserand, E. Grauges, A. Palano, G. Eigen, B. Stugu, D. Brown, M. Feng, L. Kerth, and et al., "Search for a dark photon in ee collisions at babar," *Physical Review Letters*, vol. 113, Nov 2014.

[103] E. Goudzovski, "Search for the dark photon in pi0 decays by the na48/2 experiment at cern," *EPJ Web of Conferences*, vol. 96, p. 01017, 2015.

[104] D. Curtin *et al.*, "Illuminating dark photons with high-energy colliders," *Journal of High Energy Physics*, vol. 2015, Feb 2015.

[105] P. deNiverville *et al.*, "Light dark matter in neutrino beams: Production modeling and scattering signatures at miniboone, t2k, and ship," *Physical Review D*, vol. 95, Feb 2017.

[106] A. Berlin, S. Gori, P. Schuster, and N. Toro, "Dark Sectors at the Fermilab SeaQuest Experiment," *Phys. Rev.*, vol. D98, no. 3, p. 035011, 2018.

[107] A. Berlin, S. Gori, P. Schuster, and N. Toro, "Dark sectors at the fermilab seaquest experiment," *Physical Review D*, vol. 98, Aug 2018.

[108] K. Jodłowski *et al.*, "Extending the reach of faser, mathusla, and ship towards smaller lifetimes using secondary particle production," *Physical Review D*, vol. 101, May 2020.